Chapter 3

THE DISCRETE GUST VELOCITY FIELD

It was discussed in some depth in Chapter I that the response characteristics of a flyer could only be evaluated when held directly in comparison to the nature of the disturbance environment. At a glance, the energy spectrum plotted in frequency space would, for instance, alert to any potential overlaps of energy near the natural modes of the flyer, effectively bounding analysis to energetic events within a prescribed region of interest while 'filtering' out the rest. Furthermore, a case was made that free shear layers are prevalent at, above, and within the canopied environments of interest and that the mixing layer will play a prominent role in the simulation of such flows, whether initiated along a plane or as a fundamental building block to evolve flowfields into superimposed wakes. Consider, for example, traversal through the upper canopy layer boundary of fig. 1.3 on the scale of one or a few roughness elements. Time-averaged wind variations are observed to predominantly change only with height (i.e. $\overline{\underline{u}} = \overline{u}(z)$) and wind motions relatively unencumbered by the roughness elements aloft are suddenly slowed by the momentum sink the elements represent, whereby moving from outside of the canopy layer to within (or vice versa) inflects the mean velocity profile, typically at or just above the topmost geometry of the roughness element(s). Moving from the sheltered wake of a building back into the freestream could also be described by a mean velocity profile with an inflection point. The resulting shear layer in either of these examples is the hallmark signature that a change of state in wind is occurring. Unlike the idealized step function representing the sharpest possible gradient between wind states (i.e. $\Delta z \to 0$), the friction present in the real world smoothes the gradation through the mixing process over the finite thickness of the shear layer (i.e. $\Delta z > 0$ and growing).

With the cascading nature of turbulence in mind, large energy-accepting eddies are considered coherent due to their recognizable and structured presence (i.e. able to correlated in a measured wind record) amidst an otherwise random turbulent flow field. The energy-accepting eddies of the upper atmospheric boundary layer (ABL) are not local enough (recall that $\nabla^* \sim L$ is taken as local) to directly influence the atmospheric conditions of the selected control volumes, though do indirectly contribute to the intermittency of the fluid motions as a cascaded passive background inactive turbulence. Proximate to the roughness element(s), one candidate energy-accepting (i.e. measurable) eddy length scale persists in our view, that approximated by the shear layer thickness.

In this chapter, planar mixing layers initiated across a multi-source wind tunnel without the use of a splitterplate geometry will be explored in depth. The baseline characteristics will be compared to more conventional and canonical dual-stream mixing layer experiments. This provides the basis for use of shearing velocities at the fan array exit plane to generate relevant flowfields in physical space, including the potential for planar mixing layers to be used as a simulated environment of the free-flying flyer traversing through zones of high local shear rate. To conceptually frame traversal through a mixing layer as a physical approximation of a step-forcing-function from the perspective of the flyer, a quick commentary regarding dynamic couplings is warranted.

3.1 Dynamic 'couplings' within a free shear layer

Because the free shear layer is of finite thickness, the internal dynamics must be considered when passing through. Energy-accepting eddies of a measurable size are convected with regularity at a velocity proportional to the velocity difference as they emanate from a vortex-producing source. As such, a length-scale, frequency, and velocity associated with the free shear layer itself emerge and must be held in comparison to the flyer characteristic length scale, natural modes, and performance limitations. If of similar size, characteristic frequency, or velocity amplitude, certain couplings may exist and treatment of the forcing as a step-input may no longer be justified. A fuller picture emerges when considering the wave-like nature of encountered disturbances. If, for the moment, it is supposed that generic disturbances of a certain amplitude are well-described as wave-like, then a characteristic frequency (i.e. inverse period) and convective velocity are sufficient to describe a perceived wavefront separation. Flowfields well-described by Taylor's frozen turbulence hypothesis may further be considered in the wavenumber domain and both a convective velocity and inverse wavelength associated with the flowfield more readily enter the analysis.

It is illustrative to treat each of the frequency, velocity, and length scales in turn so that metrics to evaluate performance may ultimately be established when undertaking free flight experiments within mixing layer-type disturbance environments. If, for instance, the instability frequency of the shear layer approaches the natural frequency of the flyer (i.e. frequency-coupled), a resonant response that would likely result in loss of control would be expected. A standard control dynamics analysis typically considers this. Further complications can arise for flyers near the surface however, where gust encounters are likely to be the same order of magnitude as the flyer's maximum flight speed. Instances such as these are considered to be velocity-coupled when gust ratios (i.e. the magnitude of the gust normalized by the relative freestream velocity) are $O(1)$ and signal likely saturation of control inputs. Lastly, when coherent structures comprising a mixing layer are comparable in size to the characteristic flyer length scale, then a pseudo-type gust encounter can be experienced. When the vortex core is aligned along the lifting surface, large variations in lift would be expected. Where the coherent structures may be length-coupled to the flyer, as could happen in a vortex gust encounter, the spatial distribution of velocity across the geometric lifting surfaces would need to be considered in addition to the magnitude of the event. Geometric length-couplings like these may impact stability and handling of the flyer passing through. See fig. 1.11 for a diagrammatic overview of various gust types.

If there is no significant energetic overlap of the internal dynamics of the shear layer with the response characteristics of the flyer, then treatment of the system as a flyer moving from one wind state to another is justified (a similar argument was made in justifying use of a Reynolds decomposition of the velocity field when a spectral gap is present). As a general rule, if the eddy length scales of the shear layer itself are about an order of magnitude smaller or larger than the characteristic length scale of the flyer and if the large eddy mean deformation time scale present in the shear layer flow (i.e. the time scale that governs the linearly-unstable dynamics of the large structures of the shear layer) is much shorter or much longer than the natural period of the flyer, the dynamics of the flyer can be considered decoupled from the dynamics of the shear layer, where traversal of the shear layer by the flyer can be treated as a change in wind state that occurs upon piercing the dividing streamline of air masses of two different velocities. When the velocity gradient is large (i.e. the shear layer thickness is small relative to the flyer), a flyer passing through experiences what amounts to a gust, as discrete as nature allows. In such instances, the effect of the aerodynamic forcing of the discrete gust is a function solely of the amplitude of the gust front, as is most likely to occur in the transverse and streamwise gust encounter cases. Provided the geometry is simple and the flyer of interest is at least an order of magnitude smaller than the shear layer generating geometry, the gust front can reasonably be considered in a two-dimensional planar framework when aligned with the prevailing wind. Canonical treatment of the two-dimensional free shear layer is explored next.

3.2 Turbulent free shear flows - the mixing layer

In general, turbulent free shear flows are Re-number independent with a mean velocity profile of at least one inflection point (i.e. Rayleigh-unstable) with the primary instability mechanism by vortical induction. The basic vorticity field of the mean flow determines its expected behavior and evolution in space. Nearly all flowfields with both signs of vorticity (e.g. jets/wakes) are likely to develop into a three-dimensional global structure. Unique amongst the class of turbulent free shear flows are the one-sided vorticity-distributed flowfields (i.e. mixing layers) which recover and maintain a quasi two-dimensional global structure that persists at high Reynolds numbers even in the presence of strong initial three-dimensional disturbances (e.g., see Breidenthal, 1980). Freely evolving coherent structures organize as fairly two-dimensional "rollers" in the case of a mixing layer as a consequence of a Kelvin-Helmholtz instability. The interface between rotational and irrotational fluid is intermittent so classifying an "edge" is challenging without some level of subjectivity on account of the unsteadiness. When averaged over many instantaneous realizations, a linear growth rate of the large coherent structures has been well-established. Indeed, Brown and Roshko (2012) argue that the growth rate of the mixing layer thickness is its key defining parameter.

Anatomy of a dual-stream mixing layer

A dual-stream mixing layer consists of two streams of nonzero but different velocities. The idealized step-like separations cannot exist in the real-world since mass, momentum, and energy are exchanged across the shear layer. The shear layer width, $\delta_\omega(x)$, grows with downstream development due to entrainment and typical velocity profiles evolve like that of fig. 3.1.

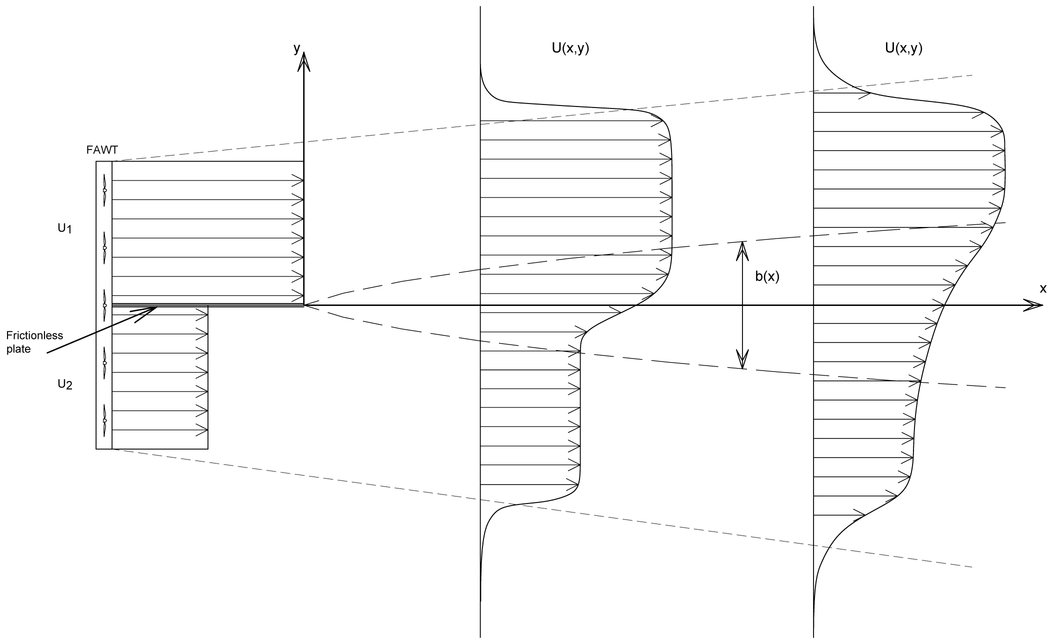

Figure 3.1: Diagram for the evolution of the mean velocity profile for a dual-stream planar mixing layer.

A mixing layer can be characterized by its velocity ratio, $r = U_2/U_1$ where U_1 is the high side freestream mean velocity and U_2 is the low side freestream mean velocity. When far enough downstream, an ideal mixing layer will reach a self-preserving state, whereby the mean velocity profiles and turbulence characteristics are self similar when scaled by a single characteristic length and velocity, typically selected to be the shear layer width $b(x)$ and the velocity difference $\Delta U = U_1 - U_2$, respectively. The mixing layer thickness is expected to grow linearly and its turbulence profiles exhibit Gaussian-like behavior, a result that can be obtained analytically from eddy-viscosity models.

Shear layer instabilities - coherent structures

The underlying structure of mixing layers was quite mysterious until the seminal work of Brown and Roshko (1974) visualized the presence of large coherent structures. These large-eddy structures were found in a turbulent dual-stream mixing layer at high Reynolds number ($Re_x = 0.5 \times 10^6$) spanning the entire mixing region, appearing to be two-dimensional in nature, persisting for longer than any apparently relevant time scale. These coherent structures are found to persist even in the presence of strong external disturbances (e.g., see Wygnanski et al., 1979) and are therefore considered to be essentially two-dimensional features of a mixing layer in the range of Reynolds numbers tested ($\sim 10^4 - 10^7$). The mixing layer grows as fresh freestream fluid is entrained into the coherent structure as it convects downstream. The velocity difference puts into motion the process described below:

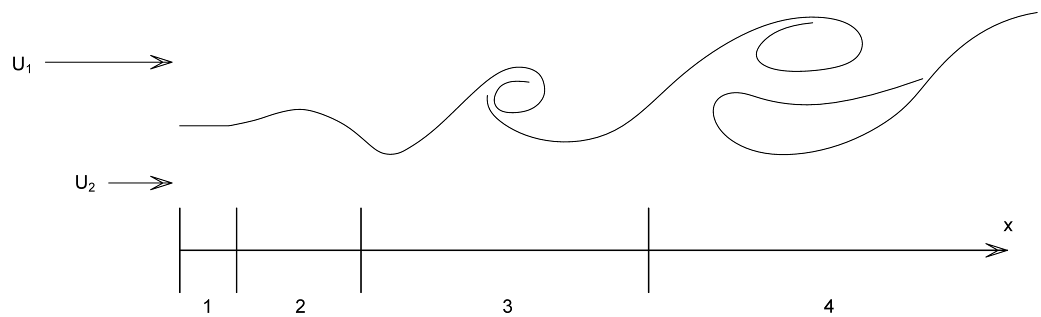

Figure 3.2: Developmental stages of a shear layer rollup.

- 1. Origin of the shear.
- 2. Fundamental Kelvin-Helmholtz instability begins to exponentially grow.
- 3. Growing disturbances cause the shear layer to roll up into discrete vortices. These spanwise rollers convect downstream and grow through entrainment.
- 4. Discrete vortices are moved from the centerline by local instabilities and begin rotating about each other, beginning to merge through a process called pairing. The amalgamation of eddies results in fewer and greater-spaced large coherent structures with downstream development.

Dimotakis and Brown (1976) showed that the entrained fluid remains discernible and practically unmixed for the lifetime of the large irrotational structure, until it rapidly mixes down to small scales. Expressed in diagram form, the coherent structures are slightly tilted downstream with a thickness, core area, and circulation that can be identified visually (e.g. from a shadowgraph or high speed video). The vorticity thickness is an approximate[1] estimate of the size of the coherent structure, denoted D in fig. 3.3.

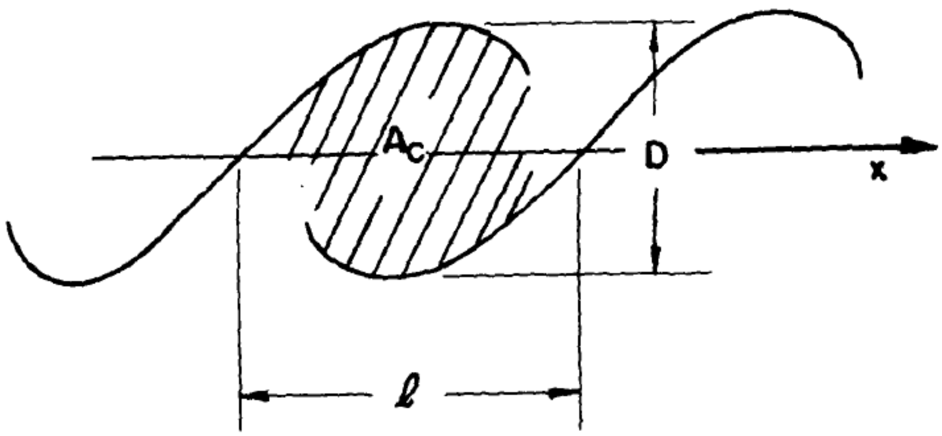

Figure 3.3: Visual properties of a large-scale coherent structure. Diagram reproduced from Bernal (1981).

3.3 Experimental mixing layers

Experimental mixing layers have traditionally been generated by single- or dual-ducted wind tunnels, separated by a splitterplate geometry with a sharp trailing edge. Much of these efforts were aimed toward establishing the self-preserving nature of these flows, understanding and subsequently amending or validating modeling efforts. This work benefits immensely from those efforts. For instance, basic criteria for describing the evolution of mixing layers is well-established and an extensive database for all such experimental shear layers (incompressible and compressible alike) can be found in the literature (e.g., see Yoder et al., 2015).

To evaluate the suitability of the experimental plane mixing layers for discrete gust testing, a shear layer characterization campaign must first be undertaken. Due to the unconventional character of the flow apparatus, in particular the absence of a splitterplate geometry coupled with a multi-source design, a rather basic analysis of the mean velocity profile characteristics is first presented followed by analysis of the turbulence characteristics to better evaluate how well multi-source generated mixing layers comport to the classical experiments.

[1]approximate because the coherent structures are quasi-regularly repeated regions of discernible correlation and are not precisely defined vortex structures as is implied in diagrammatic abstractions.

Measures of shear layer width

There exist four predominant measures of shear layer width found in the literature. Here is chosen calculation of the shear layer width $b(x)$ in three different ways, consistent with the bulk of literature on the topic. First, the shear layer width is defined using the mean velocity profile maximum slope thickness:

$$\delta_\omega = \frac{U_1 - U_2}{(\frac{\partial U}{\partial y})_{max}} \tag{3.1}$$

where δ_ω can be also interpreted as the vorticity thickness

$$\delta_\omega = |\omega|^{-1}{}_{max} \int_{-\infty}^{\infty} |\omega| \, dy \tag{3.2}$$

with $-\omega = \frac{\partial U}{\partial y}$. Secondly, a normalized form of the velocity profile, labelled herein as U^*, can be used to arbitrarily assign limits to the mixing layer:

$$U^* = \frac{U - U_2}{U_1 - U_2} \tag{3.3}$$

For instance, the location at which the normalized mean velocity profile reaches, say, $U^* = 0.05$ and $U^* = 0.95$ (i.e. 5% and 95% of its respective low and high side freestream velocities), can be denoted as $\eta_{.05}$ and $\eta_{.95}$, where $\eta = (y - y_0)/(x - x_0)$ is a similarity coordinate scaled using the downstream measurement location x and the coordinates of the virtual origin (x_0, y_0). The centerline, which can be thought of as the dividing streamline between the layers, is defined to be $\eta^* = (y^* - y_0)/(x - x_0)$, the ray on which $U^*(\eta^*) = 0.5$. This methodology is most frequently employed to determine the mean velocity characteristics of a mixing layer through the construction of spread diagrams, particularly useful when probe traversals are solely used.

Thirdly, the relevant mixing layer parameters can be calculated from an error function fit to the shape of the mean profile of the form derived by Görtler (1942). Here the normalization of the mean velocity profile is collapsed by a similarity coordinate $\xi = (y - y_0)/\delta$, which is a function solely of local shear layer conditions:

$$U^*(\xi) = \frac{1}{2}(1 + erf(\frac{y - y_{50}}{\delta})) \tag{3.4}$$

where δ is used to describe the shear layer width and y_{50}, as above, is the centerline location of the flow where $\overline{U} = \frac{1}{2}(U_1 + U_2)$.

General description of the experimental setup

The precise outer geometric dimensions $L = nd$ of the CAST FAWT used herein is 113 inches $\times$ 113 inches, though the operating envelope is conservatively taken to be 100 inches tall $\times$ 100 inches wide $\times$ approximately 250 inches long, given the individual fan-unit mixing that initializes near the fan outlet plane (see Chapter II and appendix A for more information). The dual-stream mixing layers are initiated across the 17th and 18th row of fans spanning the entire array (i.e. 113 inches) through discrete partitioning in software. The only flow manipulator installed is a honeycomb affixed directly to the face of the FAWT to eliminate the swirl of the individual fan units. This gives a nominal turbulence intensity of $3 \sim 5\%$ in the regions tested (see fig. A.10 for more information regarding the turbulence intensity distribution for this particular array). The streamwise (u) components of the velocity vector were measured at four cross-sections of the flow, starting at $x = 28$ inches and moving downstream at intervals of 30 inches, corresponding to measurement locations of $x/L \sim 0.25, 0.51, 0.77, 1.04$. A 20% spatial reduction of the testing envelope with downstream development is measured at $x/L \sim 1$ (see fig. 2.6), so that at the furthest downstream location, the measurement envelope is approximately 80 inches $\times$ 80 inches, or $\pm$ 40 inches from the tunnel centerline coordinates. Each traverse consisted of at minimum $\sim$ 30 transverse records sampled at 1kHz for 32 seconds using one single-wire hotwire.

Dual-stream mixing layer development

The mean velocity profiles in dimensional y-coordinate space are shown in fig. 3.4 for $r = 0.4$ and $r = 0.2$, with $r = U_2/U_1$, each measured at four downstream locations. Immediately evident in the dimensional view is a series of velocity overshoots and undershoots about the average respective freestream velocities, consistent with the views of fig. 2.5 and fig. 2.6 presented in Chapter II. Similar overshoots of the mean velocity profiles in traditional splitterplate dual-stream mixing layers have been reported in the near-region development on the low velocity side on account of the wake (e.g., see Mehta, 1991), but the overshoot quickly converges to the freestream velocity further downstream. Measurements in this case were taken far enough downstream to be free of any wake deficit at flow initiation due to the annular output of the individual fan units, but still within the developing region of the roughly nine inch peaked nonuniform flow behavior of the modules at all four measurement locations. The effect diminishes further downstream, as seen by tracking the maximum overshoot and undershoot deviation, as in fig. 3.5.

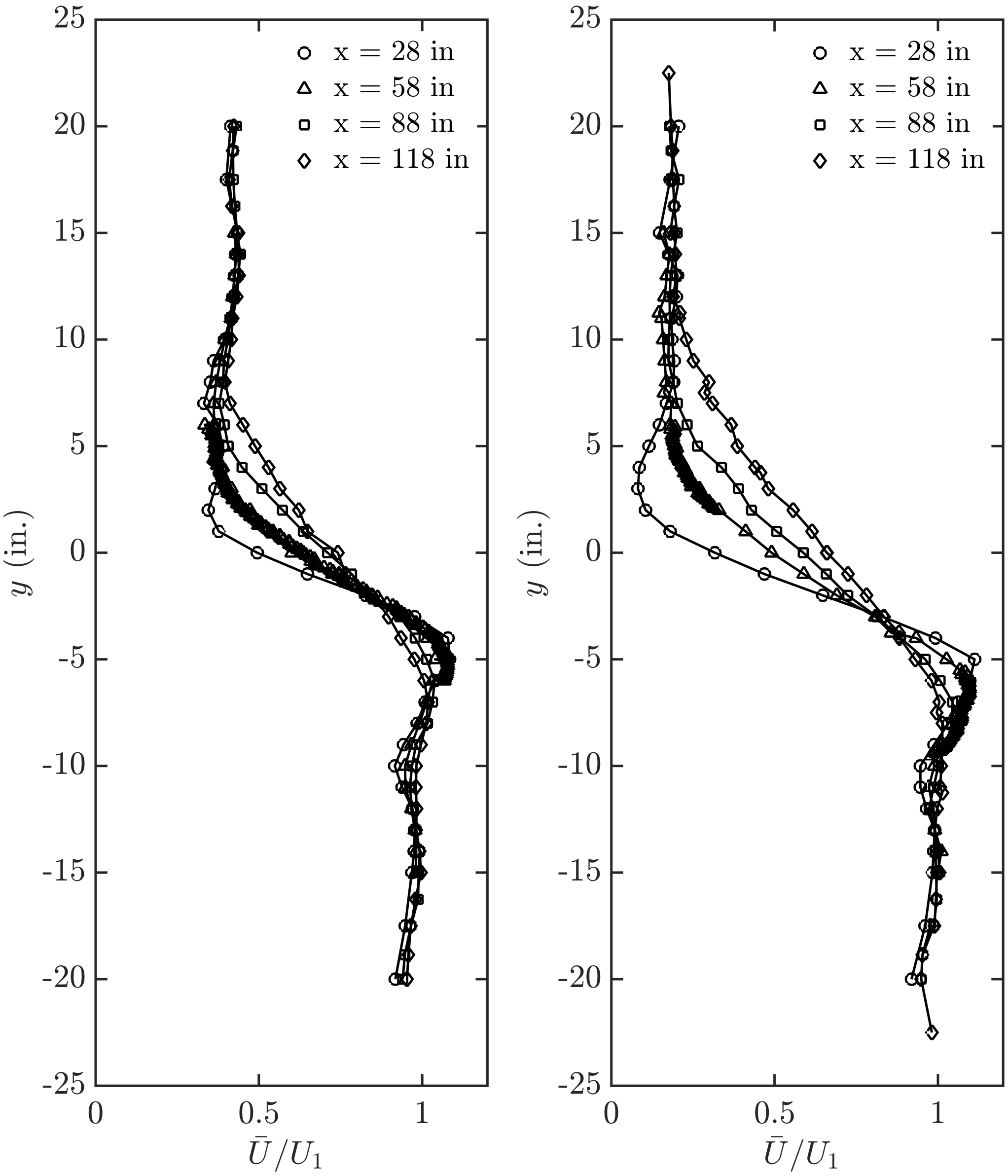

Figure 3.4: Mean velocity profiles in dimensional y-coordinate system, $r = 0.4$ (left) and $r = 0.2$ (right).

The vorticity-thickness spreading rate $\delta'_\omega = \delta_\omega/(x - x_0)$ for $r = 0.4$ and $r = 0.2$ is plotted in Figure 3.6. Due to a relationship put forth by Abramovich et al. (1984) and Sabin (1965), it is customary to plot this type of data against $\lambda = (U_1 - U_2)/(U_1 + U_2) = \sigma_0/\sigma$, rather than r. Significant scatter is noted especially for $\lambda = 1$ but also as $\lambda \to 0$. It is reasonable to posit for two streams of equal magnitude (i.e. $\lambda \to 0$) that the growth rate of the mixing layer would tend to zero. For conventional splitterplate-generated mixing layers this is not so as the effects of

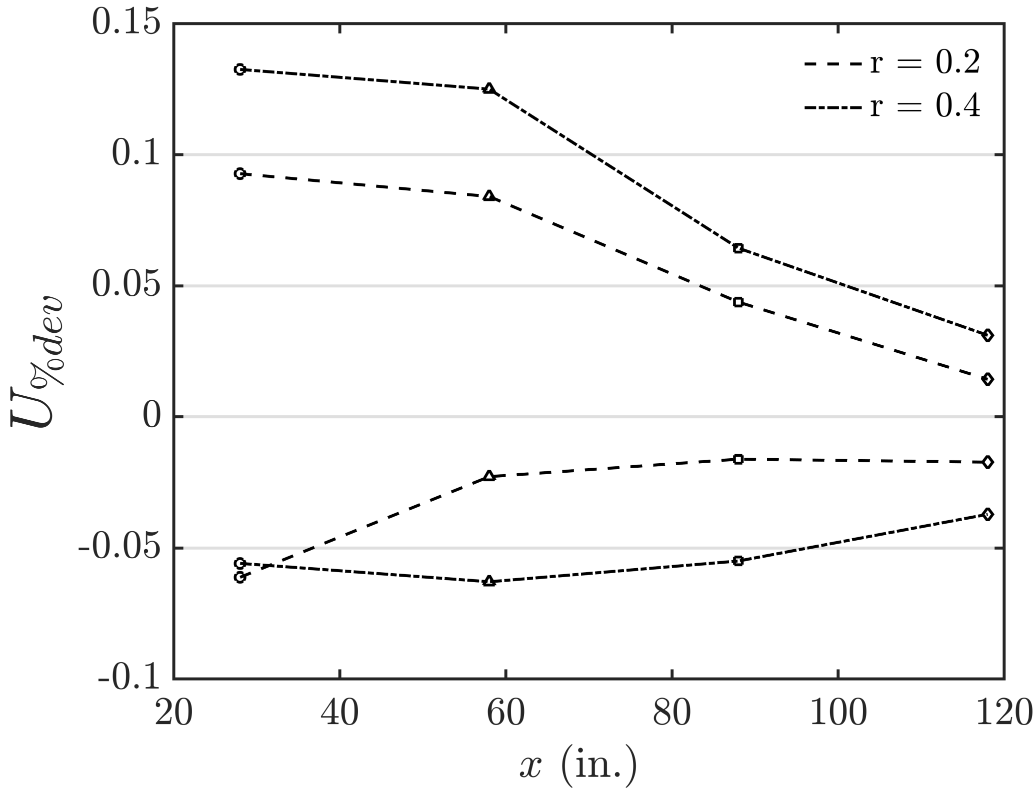

Figure 3.5: The maximum percentage velocity overshoot of the high and low side for dual-stream mixing layers generated from a modular multi-source wind tunnel.

the boundary layers developed on either side of the splitterplate persist downstream, and since the splitterplate typically spans the entirety of the test section, a wake-type flow dominates across the span of the testing domain[2]. The scatter present at $\lambda = 1$ (i.e. $U_2 \approx 0$, a single stream mixing layer) is less understood. Difficulties measuring in the low-speed side environment may contribute, though those effects are more likely to manifest in measurement uncertainties for the turbulence characteristics and not so much in the mean velocity profiles. Brown and Roshko (2012) and Suryanarayanan and Narasimha (2017) both wonder if upstream and downstream boundary conditions contribute more than has been fully recognized. The single-stream experiments of Liepmann and Laufer (1947) are typically cited as reference, where $\delta'_{\omega_0} = 0.162$ with $Re_x > 10^5$. For a greater depth discussion regarding the various proposals for the functional dependency of the spreading rate on the velocity ratio, the reader is referred to Brown and Roshko (1974).

[2]A related development was observed in fig. 2.4, but because the flow separating geometries (i.e. fan housings) are not one-dimensional (cf. thin splitterplate), the global flowfield homogenizes not too far downstream (i.e. what is called the 'uniform' flow modality).

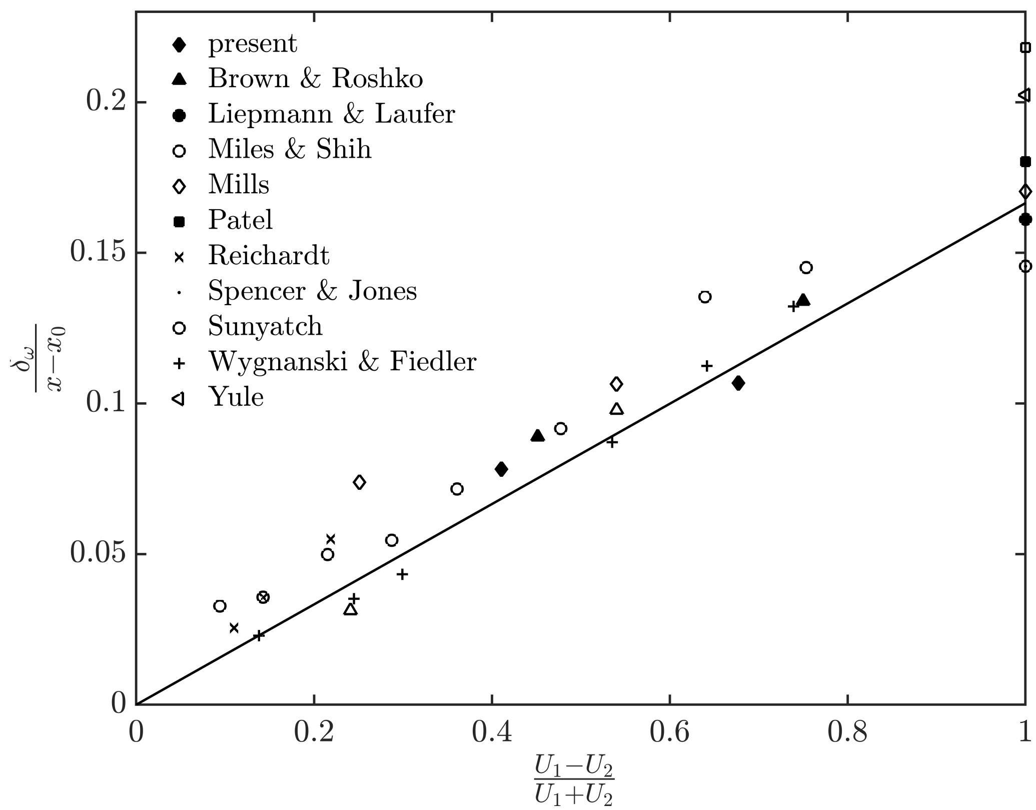

Figure 3.6: The dependence of vorticity-thickness spreading rate on the parameter $\lambda = \Delta U/2\overline{U}$ for uniform density mixing layers, as adapted from Brown and Roshko (1974) with present results added.

Absent an obvious functional relationship, a linear fit through the origin based on the present measurements is included in fig. 3.6. The linear fit intersects $\lambda = 1$ at $\delta'_{\omega_0} = 0.167$ such that

$$\delta'_\omega = 0.167\,\frac{U_1 - U_2}{U_1 + U_2} = 0.167\,\lambda \tag{3.5}$$

with r.m.s deviation = 0.0115. These results should be interpreted with some amount of caution until measurements taken further downstream over a greater variety of velocity ratios is completed. It is still believed, though, on the basis of fig. 3.6 that the mixing layers generated by the flows of this multi-source, splitterplate-less apparatus are not principally different than more conventional flow systems. Additionally it is believed that multi-source-generated mixing layers may help further the discussion regarding the asymptotic growth rate by introducing a large, high-Re, open, splitterplate-less shear-generating apparatus amenable to lab-based observation.

Some useful comparative parameters for the dual-stream mixing layers tested are summarized in table 3.1 with comparison to a select few other investigators included for additional context in table 3.2. Here $x^* = \lambda x_{max}$ is the maximum measurement location of a given experiment scaled by its velocity ratio. For the mixing layers measured herein, the maximum measurement location downstream was $x = 118$ inches, or very nearly 3000 mm. The Reynolds number is calculated from x^* and the velocity difference ΔU. The values for σ_0 are calculated from the definition of the velocity ratio, where the dual-stream spreading parameter σ is calculated from an error function fit to the mean velocity profile to be consistent with those reported in the literature.

Table 3.1: Summary of results for the dual-stream mixing layer experiments.

r	x (in)	δ_ω (in)	δ'_ω	Re_x	Re_{δ_ω}
0.4	28	3.9	0.090	$0.4 \cdot 10^6$	$0.5 \cdot 10^5$
0.4	58	5.5	0.075	$0.8 \cdot 10^6$	$0.8 \cdot 10^5$
0.4	88	8.6	0.083	$1.1 \cdot 10^6$	$1.1 \cdot 10^5$
0.4	118	10.4	0.078	$1.4 \cdot 10^6$	$1.3 \cdot 10^5$
0.2	28	4.9	0.120	$0.5 \cdot 10^6$	$0.9 \cdot 10^5$
0.2	58	8.3	0.117	$1.1 \cdot 10^6$	$1.6 \cdot 10^5$
0.2	88	10.7	0.107	$1.6 \cdot 10^6$	$1.9 \cdot 10^5$
0.2	118	13.9	0.107	$2.0 \cdot 10^6$	$2.4 \cdot 10^5$

Table 3.2: Selected parameters of comparable mixing layer experiments.

Researcher(s)	r	λ	x^* (mm)	Re_x^*	σ_0
Liepmann and Laufer (1947)	0	1.0	900	$0.9 \cdot 10^6$	11.76
Dougherty (present)	0.2	0.67	2000	$1.4 \cdot 10^6$	12.45
Dimotakis and Brown (1976)	0.2	0.67	600	$3.0 \cdot 10^6$	9.87
Spencer and Jones (1971)	0.3	0.54	680	$1.0 \cdot 10^6$	12.31
Oster, Wygnanski, et al. (1977)	0.4	0.43	470	$0.3 \cdot 10^6$	10.81
Dougherty (present)	0.4	0.43	1200	$0.6 \cdot 10^6$	11.08
Mehta (1991)	0.5	0.33	880	$0.9 \cdot 10^6$	10.5
Spencer and Jones (1971)	0.6	0.25	320	$0.3 \cdot 10^6$	13.14

Triple-stream mixing layer development

To better understand how one-sided vorticity fields generated by this multi-source apparatus evolve, an inter-shear spacing parameter is introduced to partition the fan array into three planar segments. This flow modality, referred to as the triple-stream mixing layer herein, like all other flowfields so far discussed is initiated solely through reconfigurations of software. The thickness of the middle segment is systematically increased by an even multiple of fan rows (and the relative thicknesses of the outer segments reduced by half that multiple, respectively) to observe the behavior of initial mixing and subsequent merging of the two mixing layers when sufficiently initially separated. The mixing layer with the greater velocity difference between its faster and slower freestreams is denoted as the ‘upper’ mixing layer and the mixing layer with the lesser velocity difference as the ‘lower’ mixing layer. This is shown diagrammatically in fig. 3.7.

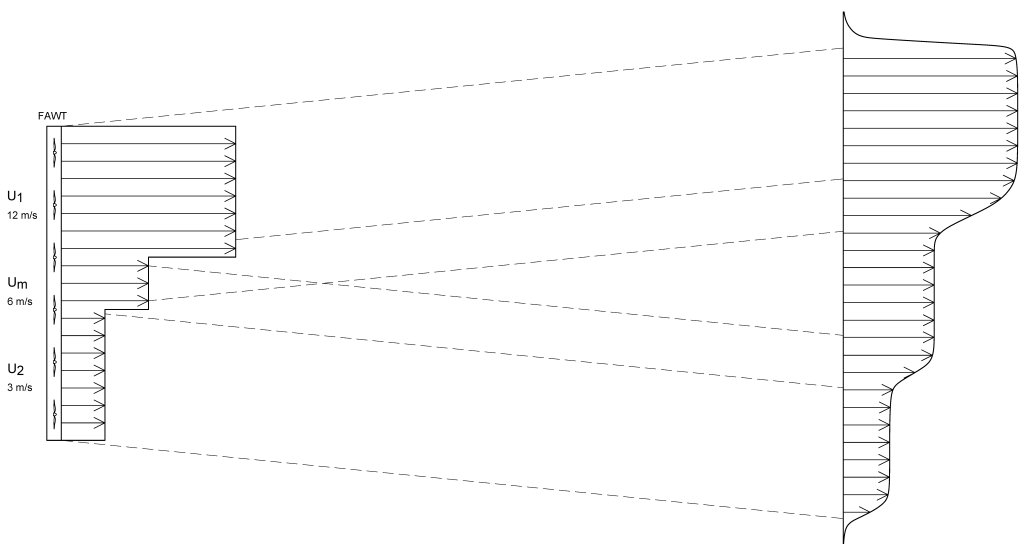

Figure 3.7: Diagram for the evolution of the mean velocity profile for a triple-stream planar mixing layer.

When the inter-shear spacing is modest, the closest analogous conventional mixing layer augmentation would be that of an increase in the splitterplate thickness, with subsequent wake dynamics shown to change the instability frequency of the flow (Dziomba and H. Fiedler, 1985). When the spacing is large enough to support two mixing layers for an appreciable distance downstream, then this is best thought of akin to a double splitterplate configuration[3].

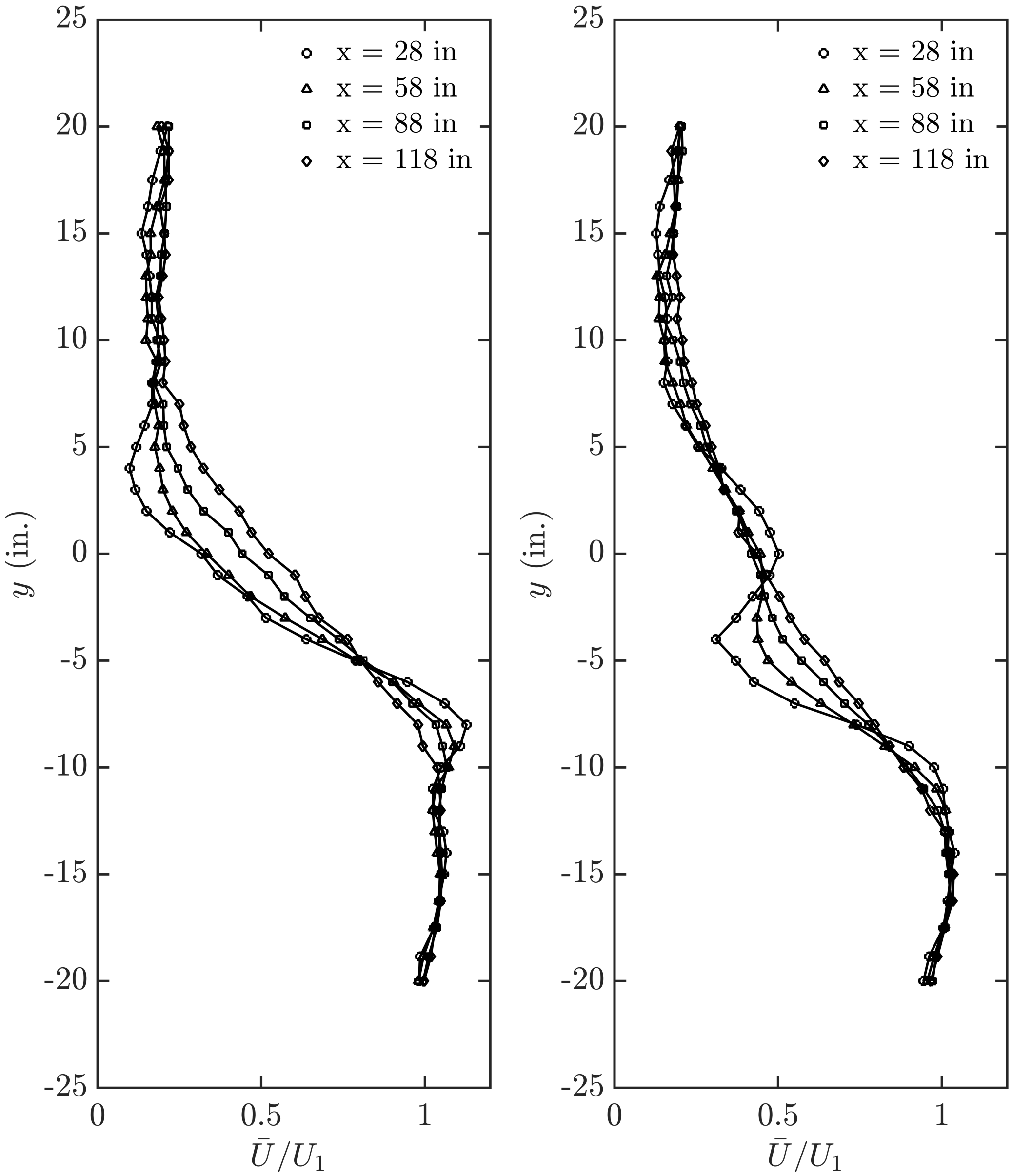

Figure 3.8: Mean velocity profiles in dimensional y-coordinate system, $r_{outer} = 0.2$, for inter-shear spacing of 6.3 inches (left) and 12.6 inches (right).

Stepping the flow in this manner may shed light on the interaction of scales within the complicated mixing layers by parsing them in a systematic way amenable to targeted studies. As a very early step toward that aim, the better-understood dual-stream mixing layer is abstracted by one dimension, introducing the aforementioned inter-shear spacing parameter as well as a merge point which describes the downstream

[3]To the best of this author's knowledge, no double splitterplate experiments have been reported elsewhere, though some work has been done in multi-jet configurations.

location where the three streams become two again. The velocity of the middle segment is theoretically initialized to divide the array to produce two mixing layers of the same velocity ratios (i.e. $r_{upper} = r_{lower}$), but with different respective velocity differences, ($\Delta U_{upper} \neq \Delta U_{lower}$).

In practice, verification of these upper and lower mixing layer velocity ratios is difficult when the two mixing layers are close to one another, since there is not a clear distinction between the low-speed stream of the upper mixing layer and the high-speed stream of the lower mixing layer. When the mixing layers have merged, an 'outer' parameterization is instead used to calculate a velocity ratio. The first triple-stream implementation presented initializes a middle segment with thickness of two rows of fan units, or $ss = 2d$, with $d = 0.080$ m being the outer dimension of the fan unit (see fig. 2.1). The velocity ratio based on the outer streams is $r_{outer} = 0.2$. The effect of the $ss = 2d$ separation is observed at the $x = 28$ inches measurement distance, whereby the vorticity thickness at that station is 55% thicker, but recovers to nominal values at subsequent measurement stations when compared to the dual-stream equivalent (i.e. $r = 0.2$ with a separation distance of $ss = 0$). These comparison results are presented in table 3.3. The x-derivative of the vorticity thickness, a measure of spreading rate, also converges to nominal values with further development downstream. The second triple-stream implementation presented increases the middle segment to $ss = 4d$. As will be more clearly evident in the geometric spreading diagrams of subsequent sections, the two mixing layers are sufficiently separated at the fan outlet plane to develop independently through much of the measurement domain. It is then possible to parse the streams and tabulate values for the upper and lower mixing layers, as has been done in table 3.4.

The goal to initialize the upper and lower mixing layers at the same velocity ratios but with nonequal velocity differences is nearly achieved up to the $x = 28$ inches measurement location. Here, $r_{upper} = 0.34$ and $r_{lower} = 0.33$, with an upper mixing layer Reynolds number based on the velocity difference and downstream location double that of the lower mixing layer (i.e. $\Delta U_{upper} = 2 \cdot \Delta U_{lower}$). Unlike the $ss = 2d$ case, the triple-stream does not recover nominally to the dual-stream characteristics within the domain tested. Indeed, the mean velocity profiles of fig. 3.8b show the tendency of the two layers to converge toward a single velocity profile maximum-slope thickness, but maintain two identifiable maximum-slope thicknesses in the $x = 118$ inches location, suggestive that the two mixing layers have yet to merge within the measurement domain.

Table 3.3: Comparison of nominal mixing layer with velocity ratio $r = 0.2$ to velocity ratio $r_{outer} = 0.2$ initially separated by $ss = 2d$.

r	x (in)	δ_ω (in)	δ'_ω	Re_x	Re_{δ_ω}
0.16	28	4.9	0.120	$0.5 \cdot 10^6$	$0.9 \cdot 10^5$
0.18	58	8.3	0.117	$1.1 \cdot 10^6$	$1.6 \cdot 10^5$
0.19	88	10.7	0.107	$1.6 \cdot 10^6$	$1.9 \cdot 10^5$
0.19	118	13.9	0.107	$2.0 \cdot 10^6$	$2.4 \cdot 10^5$
r_{outer}	x (in)	δ_ω (in)	δ'_ω	Re_x	Re_{δ_ω}
0.21	28	-	-	$0.4 \cdot 10^6$	-
0.21	58	8.3	0.123	$0.9 \cdot 10^6$	$1.2 \cdot 10^5$
0.19	88	11.0	0.113	$1.5 \cdot 10^6$	$1.9 \cdot 10^5$
0.19	118	14.3	0.113	$2.0 \cdot 10^6$	$2.4 \cdot 10^5$

Table 3.4: Summary of results for triple-stream mixing layer experiments. The two mixing layers are initially separated by $ss = 4d$ at the fan outlet plane.

r_{outer}	x (in)	δ_ω (in)	δ'_ω	Re_x	Re_{δ_ω}
0.16	28	-	-	$0.5 \cdot 10^6$	-
0.17	58	-	-	$1.0 \cdot 10^6$	-
0.19	88	-	-	$1.6 \cdot 10^6$	-
0.18	118	21.7	-	$2.2 \cdot 10^6$	$4.0 \cdot 10^5$
r_{upper}	x (in)	δ_ω (in)	δ'_ω	Re_x	Re_{δ_ω}
0.34	28	3.9	0.064	$0.4 \cdot 10^6$	$0.5 \cdot 10^5$
0.43	58	5.8	0.066	$0.7 \cdot 10^6$	$0.7 \cdot 10^5$
0.48	88	8.0	0.067	$1.0 \cdot 10^6$	$1.2 \cdot 10^5$
-	118	-	-	-	-
r_{lower}	x (in)	δ_ω (in)	δ'_ω	Re_x	Re_{δ_ω}
0.33	28	5.2	0.155	$0.2 \cdot 10^6$	$0.4 \cdot 10^5$
0.38	58	7.1	0.112	$0.3 \cdot 10^6$	$0.4 \cdot 10^5$
0.39	88	9.1	0.097	$0.6 \cdot 10^6$	$0.6 \cdot 10^5$
-	118	-	-	-	-

A longer term general objective of multi-source fan array wind tunnel research is to model initial shear conditions between each fan unit, particularly for unsteady flow generations. One can imagine the immense task ahead to understand the mixing behavior of same- and opposite-sign turbulent flows generated from some 1296 annular outputs as they change in time[4].

[4]If one cares to indulge, this concept can be conceptually abstracted to n-dimensions, n being set by the resolution of the FAWT. Since FAWT are of finite extent, the local inter-shear spacing of each

Spreading diagrams - a geometric view

When the dual-stream mean velocity profiles are plotted in U^* coordinates, the spreading diagrams of fig. 3.9 and fig. 3.10 can straightforwardly be constructed by tracking (somewhat arbitrarily) select locations of the mixing layer. The locations at which $U^*(y_{05}) = 0.05$, $U^*(y_{50}) = 0.50$, and $U^*(y_{95}) = 0.95$ are tracked herein. The virtual origin (x_0, y_0) is determined by extrapolating the linear fits to their mutual intersection. When shifted by y_0, the centerline of the mixing layer is seen to deflect toward the low velocity side, as to be expected from the literature.

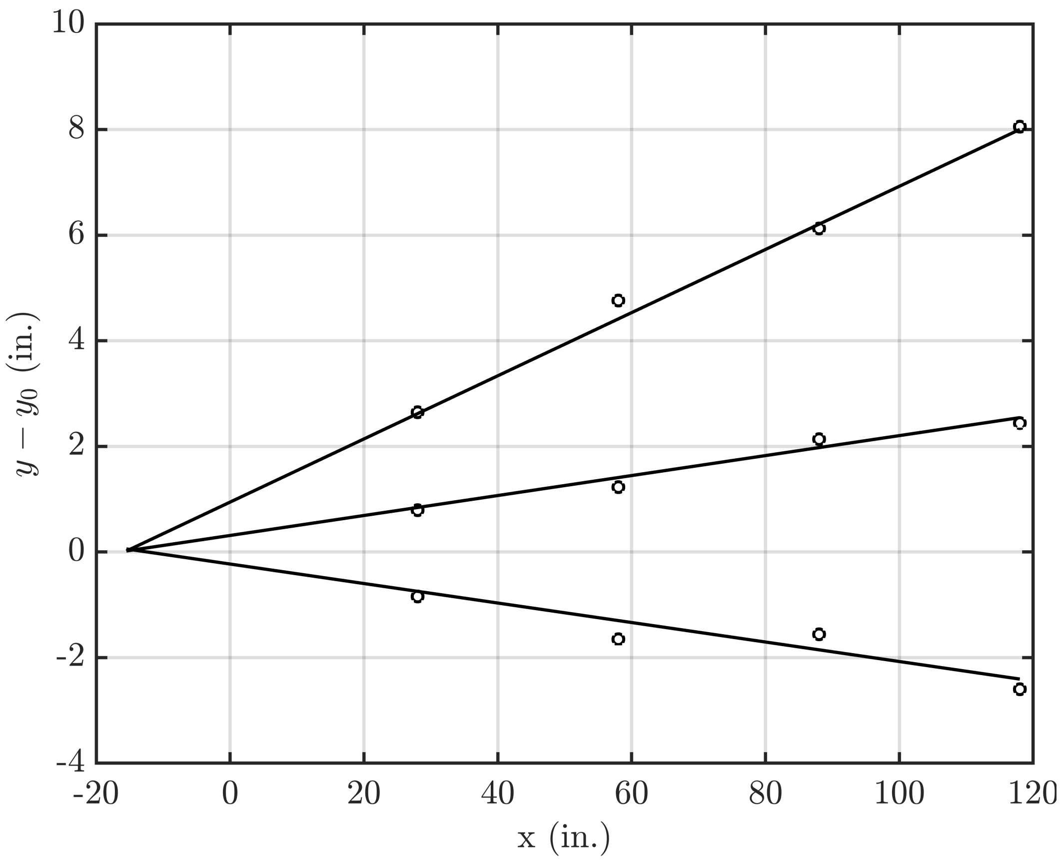

Figure 3.9: Spreading diagram for dual-stream mixing layer with $r = 0.4$.

---

mixing layer is reduced as more segmentations are added. If each stream was enforced to be of the same width, one can see how the max attainable inter-shear spacing would monotonically decrease with n, thereby reducing the maximum downstream location of the merge points and recovering the uniform flow modality.

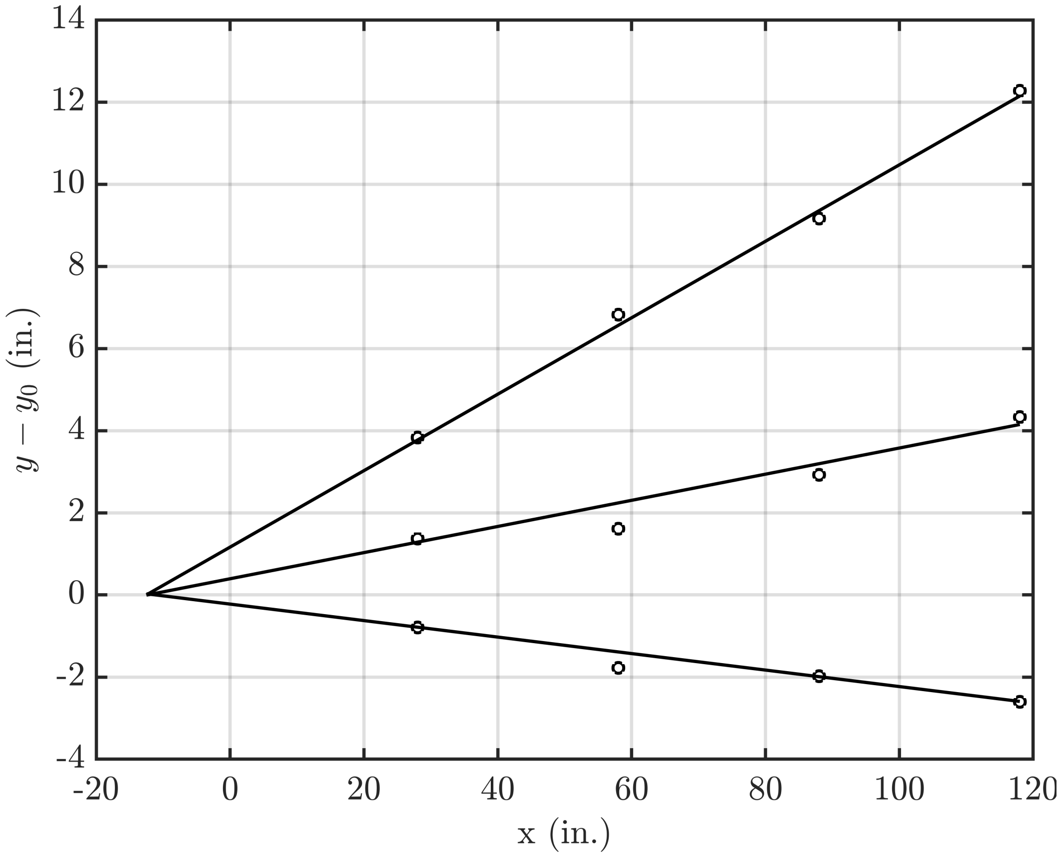

Figure 3.10: Spreading diagram for dual-stream mixing layer with r = 0.2.

Greater care is required for the triple-stream cases. As discussed previously, when the two mixing layers are separated enough to maintain a distinct middle stream, the upper and lower mixing layers can be evaluated separately. Cross markers (×) denote when a given triple-stream dataset is able to be parsed as separate mixing layers. Upper mixing layer data points are given in red and lower mixing layer data points in blue. Otherwise, outer stream parameters are used, denoted by black circle markers (o). Two new length scales are introduced when the two mixing layers of the triple-stream case develop distinctly in physical space (i.e. $x > 0$). The inter-shear spacing parameter y_{iss} is defined as the distance between the centerlines of two neighboring, same-sign vorticity, mixing layers and a geometric merging point x_{merge} can be identified as the intersection of the lines corresponding to the low-speed stream of the upper mixing layer and the high-speed stream of the lower mixing layer. Figure 3.11 combined with the tabulated results of table 3.3 suggest that the triple-stream mixing layer with an initial separation of $ss = 2d$ recovers to the nominal $r = 0.2$ dual-stream case beyond $x > 58$ inches.

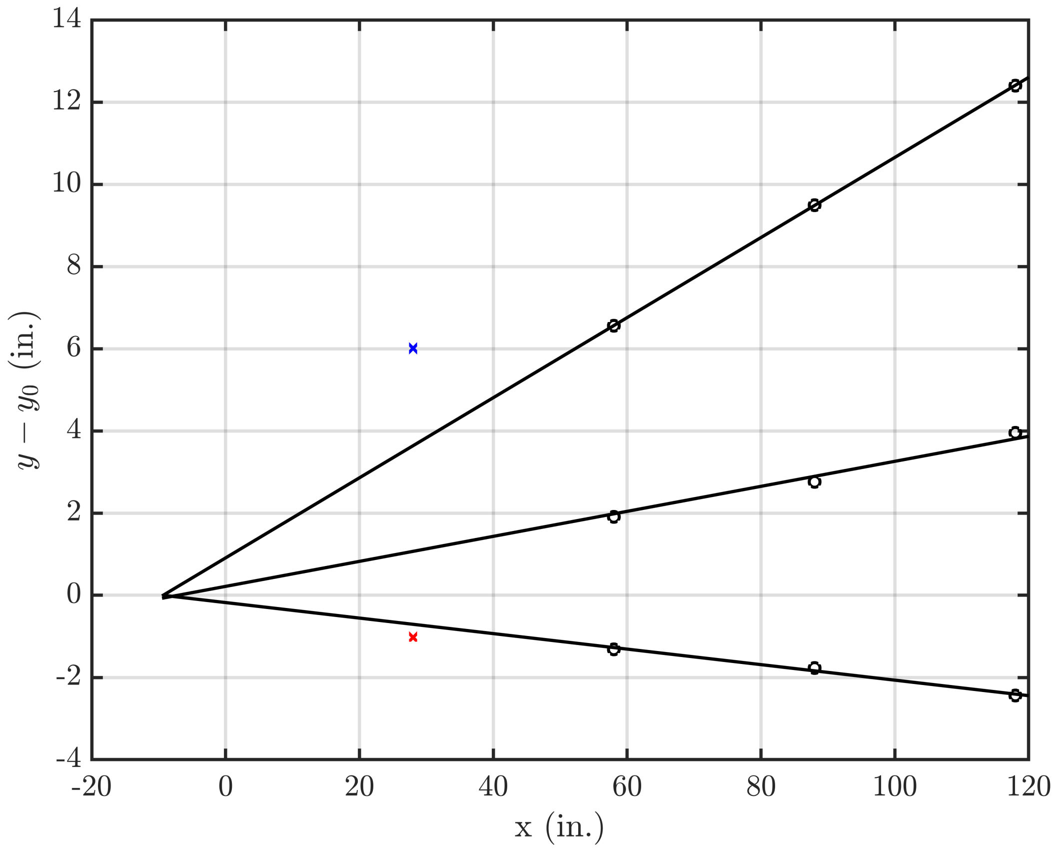

Figure 3.11: Spreading diagram for r_{outer} = 0.2 with a $2d$ initial separation at fan inlet plane.

Figure 3.12 suggests that full merging of the two mixing layers in the triple-stream case of $ss = 4d$ has not occurred within the measurement domain, but is likely to occur slightly beyond the measurement location $x = 118$ inches. Judicious choice of these two triple-stream mixing layers within the predetermined measurement domain effectively brackets the salient characteristics of merging same-sign vorticity mixing layers.

There are at least three identifiable regions in the development of the triple-stream mixing layers. First, when the two layers are sufficiently separated to develop nominally, an upper and lower mixing layer are established (termed Region I). Then, a region where the two mixing layers are still distinct but feel the effect of one another establishes (Region II) and begins to move the centerlines of the respective mixing layers closer to one another.

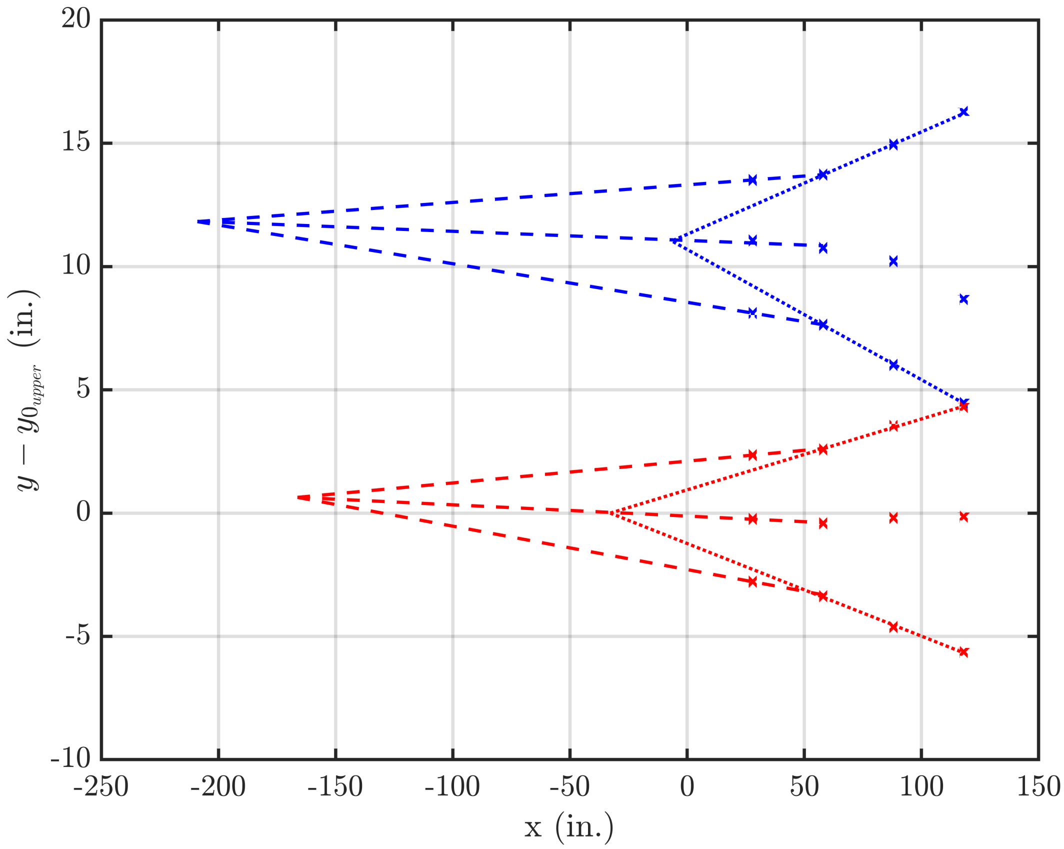

Figure 3.12: Spreading diagram for triple-stream mixing layer with a $4d$ initial separation at fan inlet plane.

The centerline of the lesser velocity difference mixing layer (lower) seemingly moves more toward the greater velocity difference mixing layer (upper), suggestive that the lower mixing layer is absorbed into the upper one. Lastly, the triple-stream mixing layer, which can begin as two distinct same-sign vorticity mixing layers, fully merges (Region III) back to a dual-stream mixing layer with outer spreading properties comparable to the nominal dual-stream case, with the exception that the vorticity thickness is necessarily increased. In fact, it is evident when comparing the outer-stream-based vorticity thickness of the $ss = 2d$ versus the $ss = 4d$ case, which has an increased initial thickness of $2d = 6.3$ inches, that the vorticity thickness at the nearly-merged furthest downstream location has essentially increased by that $2d$ amount (from $\delta_\omega = 14.3$ inches to $\delta_\omega = 20.7$ inches). The extra separation is seemingly absorbed into the dual-stream mixing layer that manifests when far enough downstream.

A geometric approximation that ignores the complexity of Region II can be a useful tool in predicting the general location at which merging is likely to occur. For instance, taking the basic structure of the initially distinct mixing layers of the $ss = 4d$ case and geometrically (artificially) moving one mixing layer closer to the other by a factor of $2d$ in fig. 3.13 gives the approximated structure of the $ss = 2d$ case of fig. 3.11 and indicates that the merging point x_{merge} would likely occur between 35 inches and 53 inches downstream.

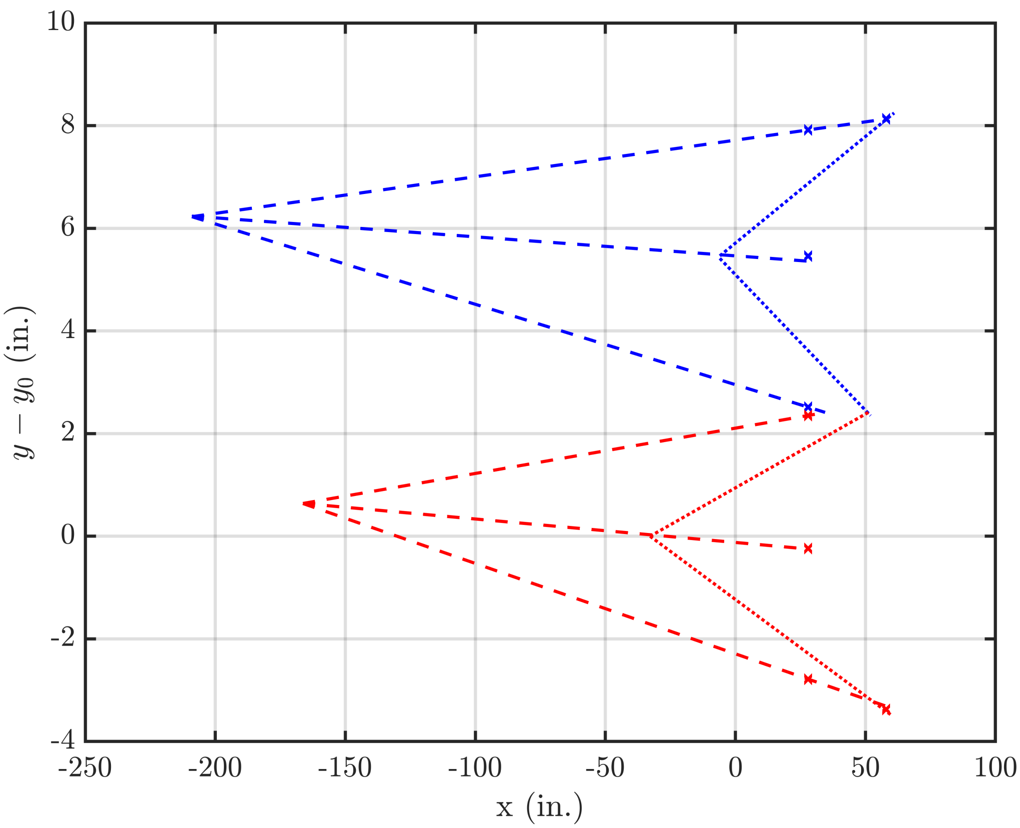

Figure 3.13: Spreading diagram for a geometrically reduced inter-shear spacing of $l_{4d}/2 = l_{2d_{art}}$.

Indeed, it can be said that for the $ss = 2d$ case, somewhere between $x = 28$ inches and $x = 58$ inches a change in spreading rate accompanies a merging point. It is reasonable to expect in the $ss = 4d$ case shortly beyond $x > 118$ inches where the triple-stream likely merges to become a dual-stream mixing layer that an increase in spreading rate would accompany the merge and begin to spread nominally. A more direct geometric comparison of the development of each mixing layer (both initiated and evolved) can be made by pinning each respective virtual origin to $y = 0$ inches and rotating the mixing layer such that the every centerline point falls along the line $y = 0$ inches, as if the mixing layers are evolving about the same dividing streamline. This representation, given in fig. 3.14, acts then as the basis of the chosen similarity coordinates in the following section, particularly for the triple-stream cases whereby portions of the development may be distinctly separate or fully merged dependent on the downstream location, initial separation distance, and relative velocity differences.

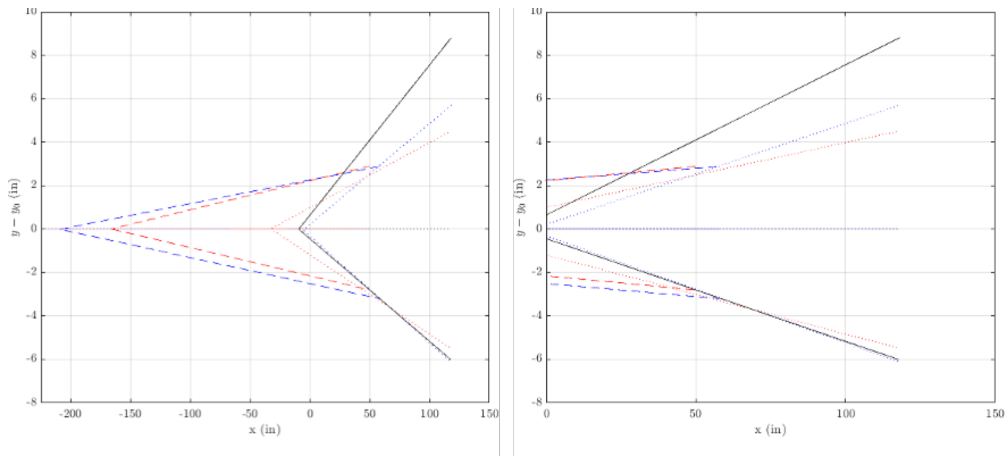

Figure 3.14: Spreading diagram for the triple-stream cases with virtual origin brought up to the line $y = 0$ inches and rotated such that every centerline point falls along the line $y = 0$ inches. The rightmost plot is a zoomed in view of the development in physical space ($x > 0$ inches). The color and line-type are as in fig. 3.11 and fig. 3.12.

Mixing layers in similarity coordinates

For a given data series, the virtual origin is determined from the spreading diagrams of the previous section. Dual-stream mixing layers have one such virtual origin so there is no ambiguity in interpretation for those datasets. Triple-stream mixing layer cases, however, manifest different spreading rates dependent on the region of development. When the triple-stream mixing layers are comprised of two distinct mixing layers (Region I), the mixing layers are analyzed separately. When the two mixing layers are beginning to merge but still maintain different maximum velocity profile slopes (Region II), upper mixing layer coordinates are arbitrarily selected for the analysis. Finally, if the two mixing layers have merged (Region III), the outer stream parameters are used. The virtual origin for the triple-stream cases can thus change for a given data series and is selected according to the appropriate ray of fig. 3.14 at each respective downstream location.

Mean velocity characteristics

Figures 3.15 to 3.19 show the normalized mean velocity profiles plotted in η coordinates, shifted by $-\eta^*$, where $\eta = (y - y_0)/(x - x_0)$ and $\eta^* \equiv (y_{50} - y_0)/(x_{50} - x_0)$. A dimensional reference is provided for the triple stream mixing layer cases. Collapse of the profiles within the mixing layer is excellent, with scatter prevalent at both low and high speed freestream sides. Since the spatial nonuniformity is roughly constant at every downstream location, normalization of the y-coordinate by any nominally increasing length parameter (downstream distance, x, in this case) will manifest as a progressive pinching of these overshoots.

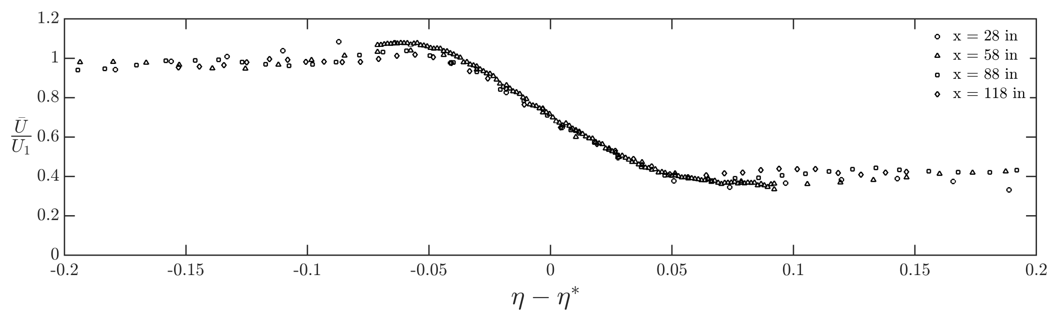

Figure 3.15: Mean velocity profiles of the dual-stream mixing layer in η-similarity coordinates, $r = 0.4$.

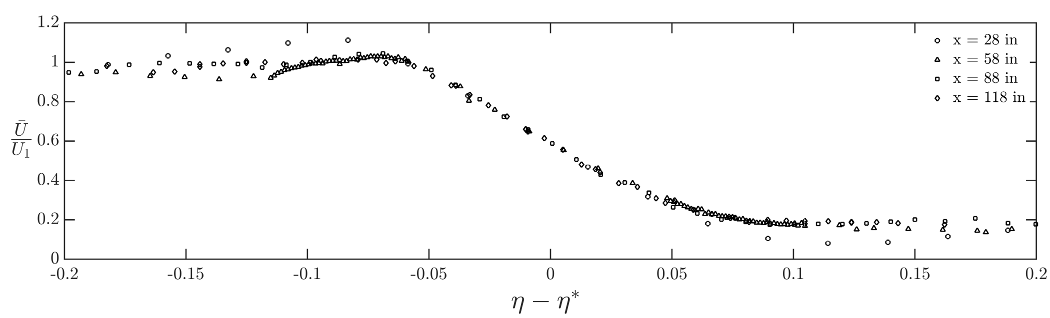

Figure 3.16: Mean velocity profiles of the dual-stream mixing layer in η-similarity coordinates, $r = 0.2$.

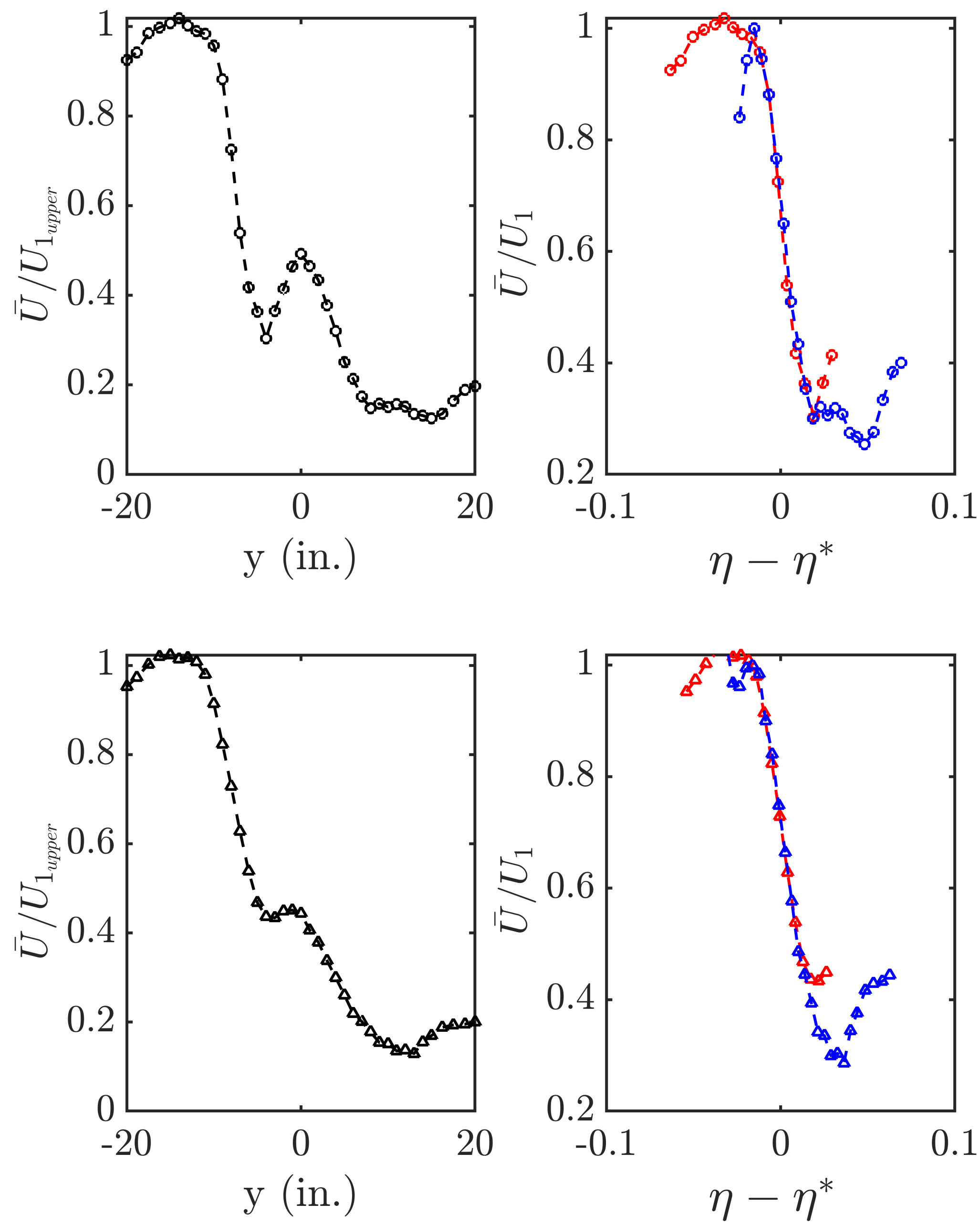

Figure 3.17: Mean velocity profiles of the triple-stream mixing layer with initial separation of $ss = 4d$ in η-similarity coordinates. The top row presents data from $x = 28$ inches and the bottom row from $x = 58$ inches. Red denotes the upper mixing layer and blue denotes the lower mixing layer. Here, the upper and lower mixing layers are distinct (region I) enough to be treated separately.

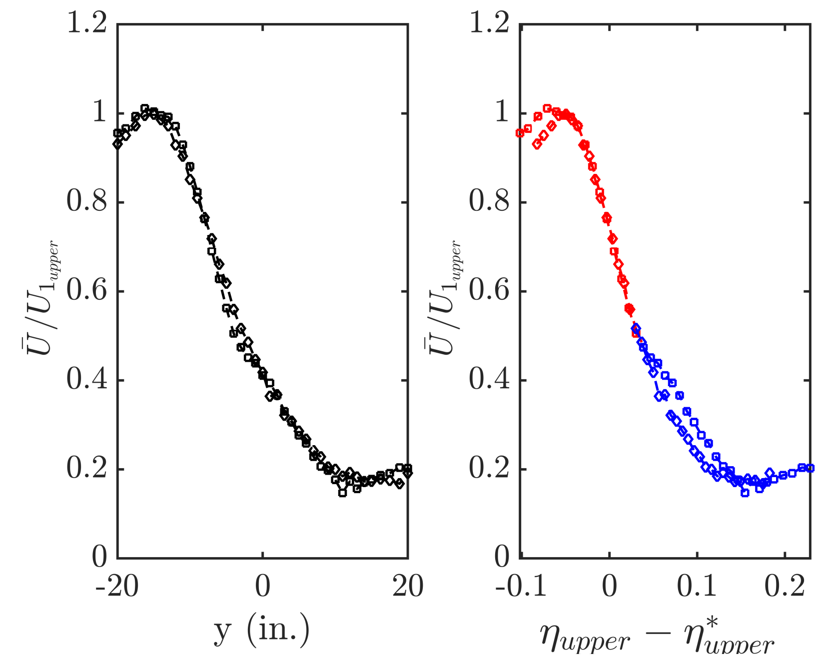

Figure 3.18: Mean velocity profiles of the triple-stream mixing layer with initial separation of $ss = 4d$ in η-similarity coordinates at downstream locations $x = 88$ inches and $x = 118$ inches. Here, the upper and lower mixing layers are transitioning towards merging (region II).

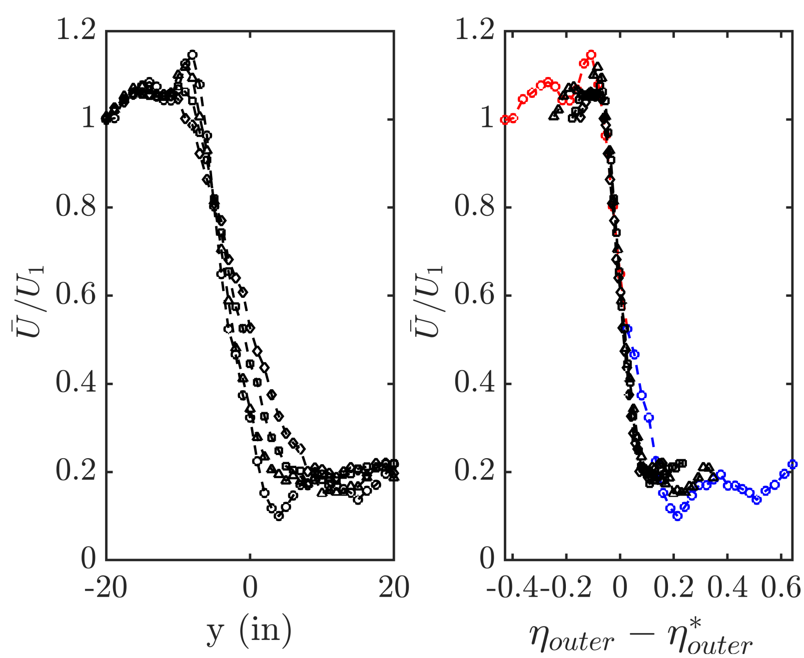

Figure 3.19: Mean velocity profiles of the triple-stream mixing layer with initial separation of $ss = 2d$ in η-similarity coordinates at. Beyond $x > 28$ inches, the upper and lower mixing layers have merged (region III) and can be treated as a dual-stream mixing layer.

Turbulence characteristics

If Re_x is sufficiently large, viscous terms in the streamwise momentum equation can be neglected to give an order of magnitude balance of the two velocity and length scales for a planar mixing layer as $u^2_{ML}/U^2_{ML} = O(l_{ML}/L_{ML})$. Taking the representative velocity and length scale in the transverse direction to be the fluctuating velocity u' and vorticity thickness δ_ω and the representative velocity and length scale in the streamwise direction as the velocity difference ΔU and distance from the virtual origin, respectively, then:

$$u'^2/\Delta U^2 = O(\delta_\omega/(x - x_0)) = O(\delta'_\omega) \tag{3.6}$$

Thus, to achieve self-preservation, the magnitude of the ratio of the fluctuating velocity and the mean flow difference must be constant with downstream development. When the fluctuating velocity is squared and normalized by the square of the velocity difference, the distribution of the streamwise normal stress is presented. The baseline turbulence intensity of the high-speed and low-speed freestream of the present experimentation is nominally 4-5 times higher than any of the incompressible, constant density experiments with comparable Reynolds number referenced by Yoder et al. (2015). The distribution of the longitudinal component of the velocity fluctuations across the mixing layers for $r = 0.4$ and $r = 0.2$ are shown in fig. 3.20 and fig. 3.21. Peak values in the present experiments, particularly for the furthest downstream locations, reside between values of 0.035 and 0.040. Spencer and Jones (1971) report for the weaker shear case of $r = 0.6$ peak amplitudes in the fully-developed regions were $(u'/\Delta U = 0.19)^2 = 0.036$. Saiy and Peerless (1978) who introduced a static grid to increase freestream turbulence intensity upwards of 5%, found similar values in their weaker shear case of $r = 0.66$. A slight proportional increase in peak values seems attributable to initial freestream turbulence values, though the effects are thought to be secondary, affecting only the three-dimensional structures riding along the basically two-dimensional coherent structures. Though the evolution of the velocity fluctuations follows closely the mean velocity profile, some of the scatter in the data, particularly at the two closest measurement locations, could be attributable to the near-region development of the mixing layers. Spencer and Jones (1971) shows that the development of the pressure fluctuations lag behind the velocity fluctuations. Future experimentation should include a companion pressure probe to narrow the location where the mixing layer becomes fully developed.

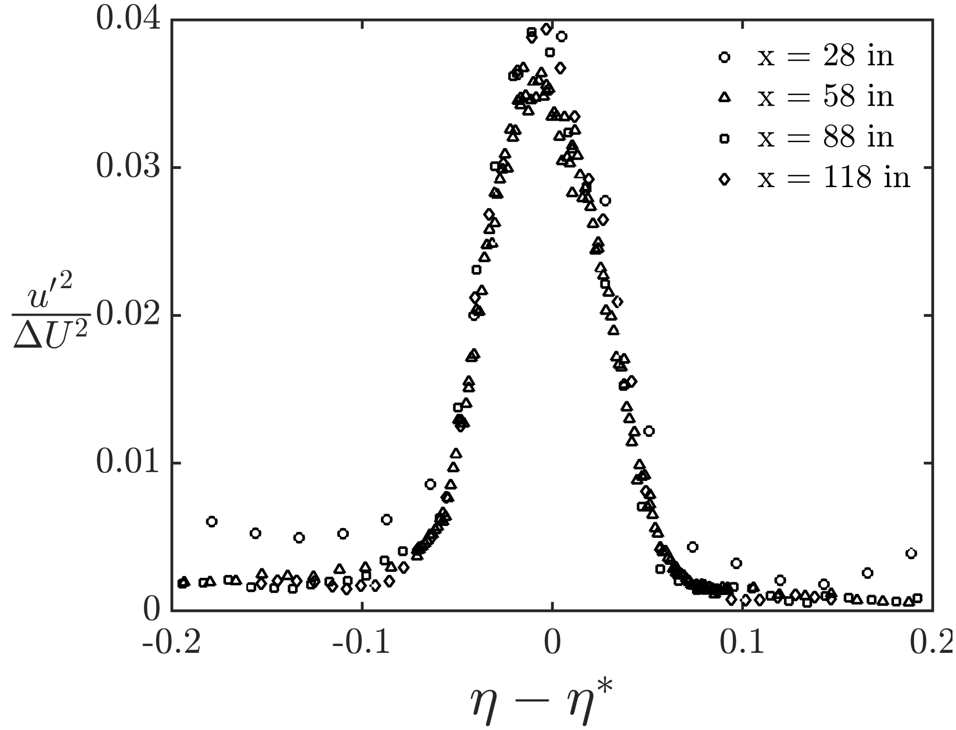

Figure 3.20: Distribution of streamwise normal stress for r = 0.4.

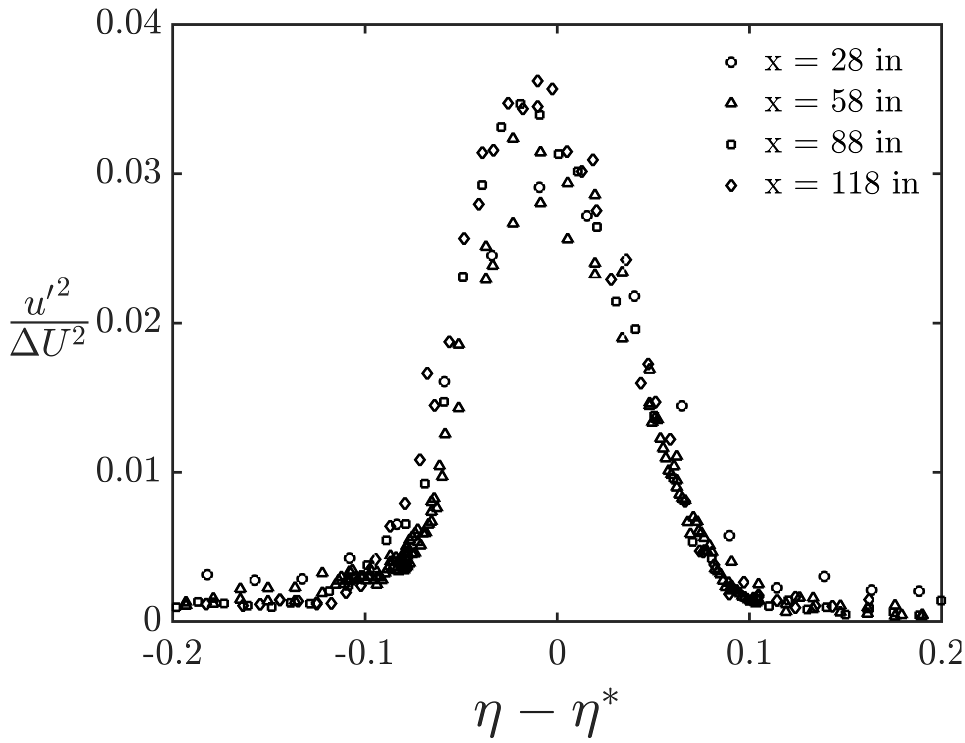

Figure 3.21: Distribution of streamwise normal stress for r = 0.2.

Both sets of velocity fluctuation distributions behave Gaussian-like with good collapse in the mixing layer region when plotted in similarity coordinates, which is ordinarily a good indicator of a fully-developed flowfield. According to the results summarized in table 3.1, values of δ'_ω are changing throughout the $r = 0.4$ case, but do seemingly converge to a nominally constant value of 0.107 for the $r = 0.2$ case. Tennekes et al. (1972) suggest, based on experiments up through the year 1972, that mixing layers become self-preserved when $Re_x > 4 \cdot 10^5$.

The methodologies used to analyze the mean-velocity profiles of the triple-stream cases discussed in the previous section are implemented for the fluctuating velocities of the triple-stream cases in figs. 3.22 to 3.24.

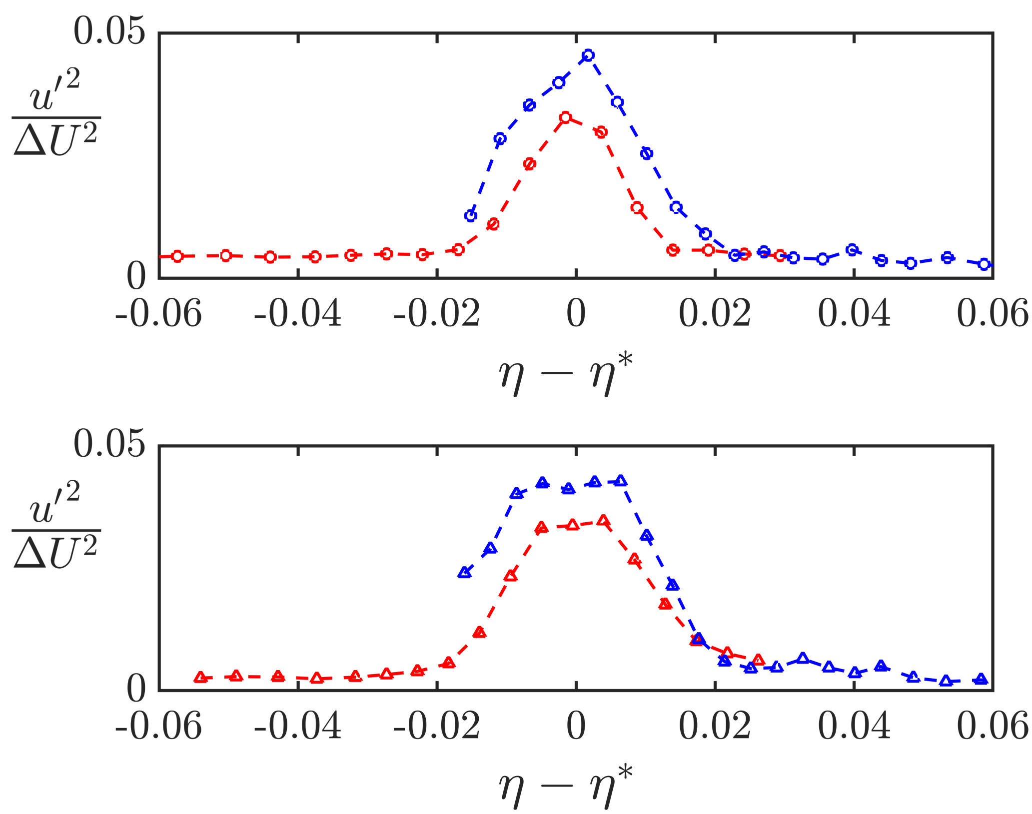

Figure 3.22: Fluctuating velocity profiles of the triple-stream mixing layer with initial separation of $ss = 4d$ in η-similarity coordinates. The top row presents data from $x = 28$ inches and the bottom row from $x = 58$ inches. Red denotes the upper mixing layer and blue denotes the lower mixing layer. Here, the upper and lower mixing layers are distinct (region I) enough to be treated separately.

Tracking the location of the peak of the fluctuating velocities sheds some light on the development of the merging triple-stream mixing layers. In the $ss = 4d$ case of fig. 3.23, where the upper mixing layer similarity coordinates are used, the upper mixing layer peak fluctuating velocity is pinned to $\eta_{upper} - \eta^*_{upper} = 0$. For $x = 88$ inches, the lower mixing layer peak fluctuating velocity is still distinct and broadly peaked about $\eta_{upper} - \eta^*_{upper} = 0.1$. However, with merging eminent just beyond $x = 118$ inches, both the lower and upper mixing layer peaks begin to move toward a new developing peak at $\eta_{upper} - \eta^*_{upper} = 0.025$. The relative movements of the peaks before and after merging are more clearly showcased in the outer similarity coordinate representation of the $ss = 2d$ case. Here, for $x = 28$ inches, the upper mixing layer peak is located at $\eta_{outer} - \eta^*_{outer} = -0.02$ and the lower mixing layer peak is located broadly about $\eta_{outer} - \eta^*_{outer} = 0.07$, suggestive that the lesser velocity difference mixing layer is absorbed into the upper mixing layer somewhere between $x = 28$ inches and $x = 58$ inches.

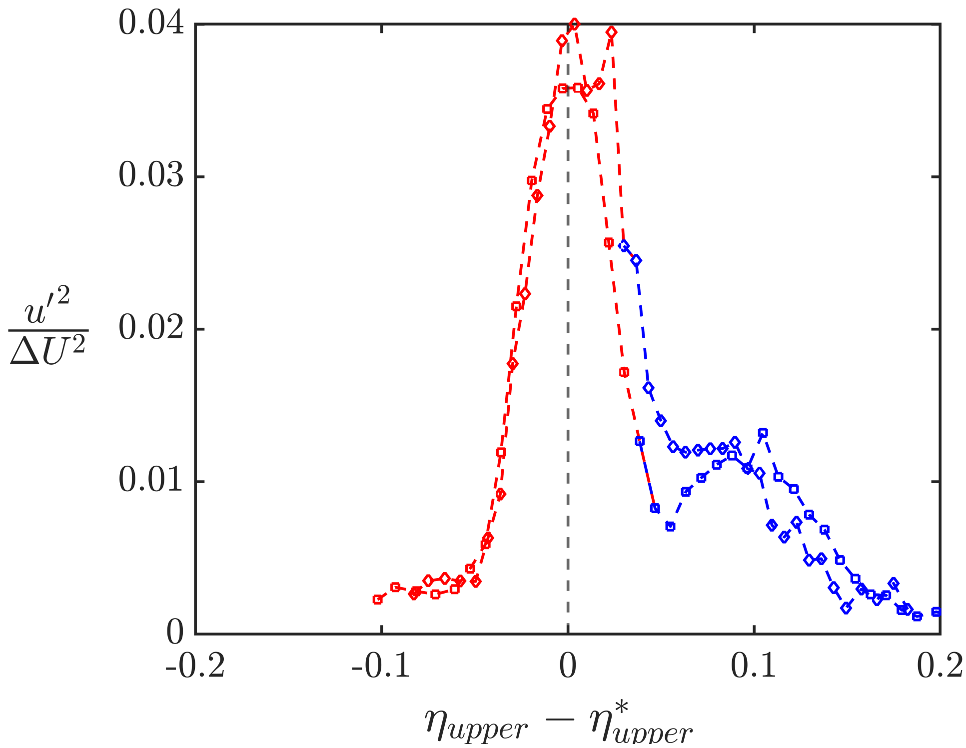

Figure 3.23: Fluctuating velocity profiles of the triple-stream mixing layer with initial separation of $ss = 4d$ in η-similarity coordinates at downstream locations $x = 88$ inches and $x = 118$ inches. Here, the upper and lower mixing layers are transitioning towards merging (region II).

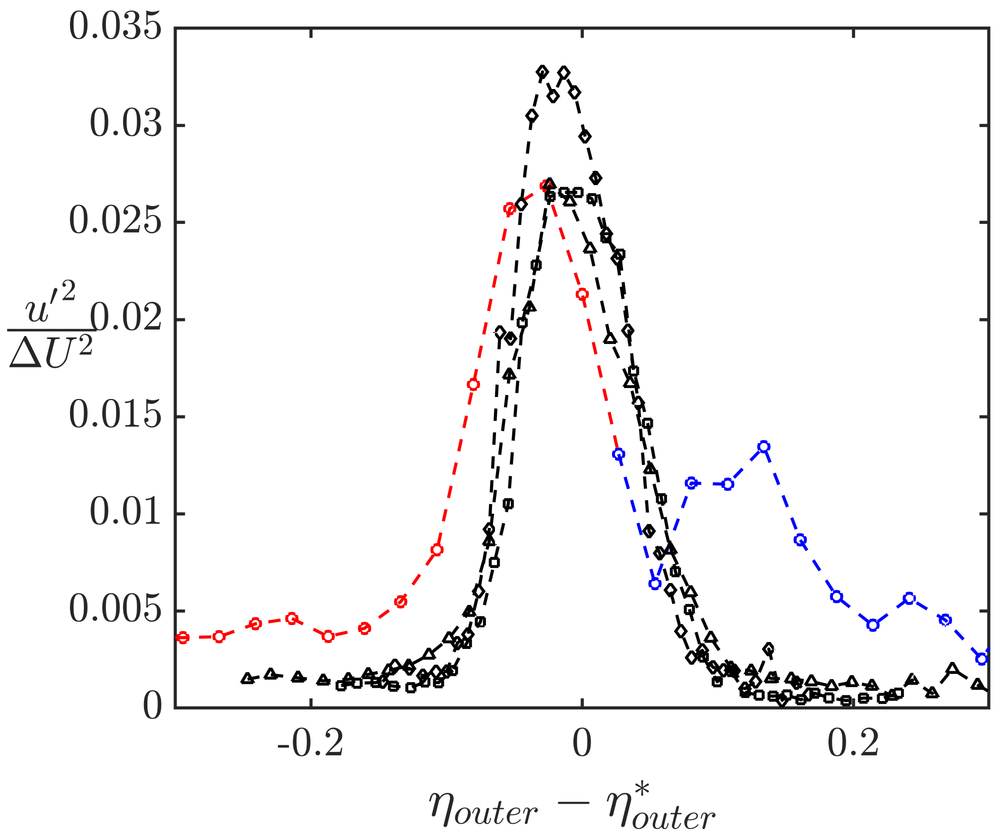

Figure 3.24: Fluctuating velocity profiles of the triple-stream mixing layer with initial separation of $ss = 2d$ in η-similarity coordinates at. Beyond $x > 28$ inches, the upper and lower mixing layers have merged (region III) and can be treated as a dual-stream mixing layer.

Measurement error - dual-stream example

The predominant source of scatter seen throughout on the low-speed velocity side of the mixing layers, but particularly for the of $r = 0.2$ cases, is believed to be measurement-based. Calibration ranging errors of the hotwire anemometer were observed to occur more frequently when the temperature dropped late at night in the semi-outdoor environment of CAST where the experiment was undertaken. The calibration procedure employed (re-calibrated for current temperature at the beginning of each night of experimentation) may not have been sufficient to track with the temperature drop over the roughly hour long data sweeps. This scatter is more readily apparent in the skewness and kurtosis distributions of figs. 3.25 to 3.28.

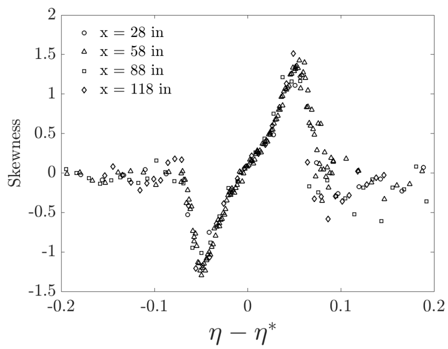

Figure 3.25: Distribution of skewness for $r = 0.4$.

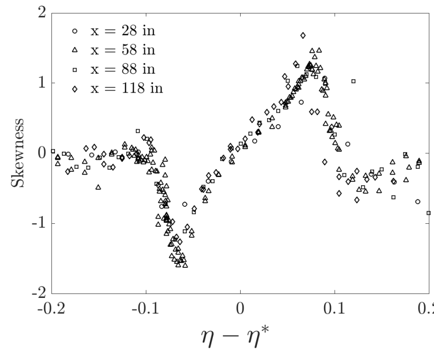

Figure 3.26: Distribution of skewness for $r = 0.2$.

The skewness factor is representative of the symmetry of the fluctuating quantities while the kurtosis is representative of the amplitude distribution with respect to the variance $\overline{u'^2}$. The u-component skewness factor curve for $r = 0.4$ (fig. 3.25) collapses nicely in similarity coordinates with an inflection in the mixing layer region, an indication of a high degree of homogeneity of turbulence in that region, but maintains significant scatter on the low-speed side. The kurtosis plots show the freestream value at approximately 3, which is consistent with the literature. The flat part of the mixing region is ~ 2.75, which is quite a bit lower. It is generally accepted that a value of 3.5 in the mixing region is indicative of a fully turbulent region. The scatter on the low side can most likely be attributed to the hotwire calibration nearing its operational limits and not necessarily an increase in intermittency as would be implied with a higher kurtosis value. Absent pressure fluctuation distributions and absent data measured further downstream, the mixing layers tested herein cannot be conclusively labeled fully-developed, though seemingly trend that way beyond $x = 88$ inches.

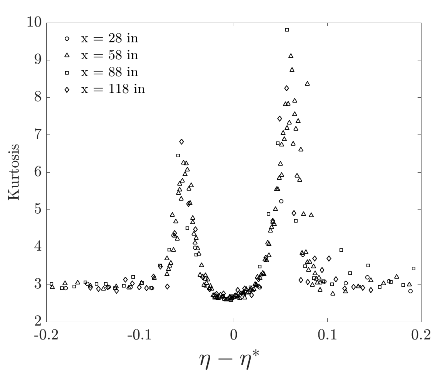

Figure 3.27: Distribution of kurtosis for $r = 0.4$.

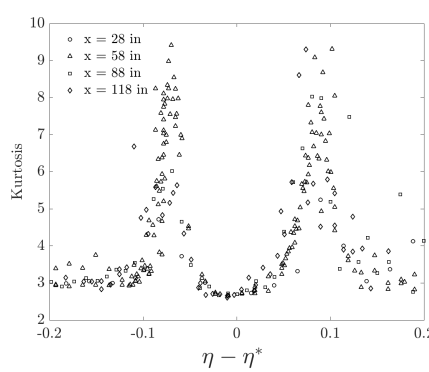

Figure 3.28: Distribution of kurtosis for $r = 0.2$.

Spectral analysis

The longitudinal u-component energy spectrum (see section 4.2 for definitions) along the centerlines of the various mixing layers (i.e. $\eta^* = 0.5$) are presented in figs. 3.29 to 3.31. A $-5/3$ region was clearly developed in every presented case, strongly suggestive of local isotropy in those regions. A coarse traverse at $x = 7$ inches for the dual-stream case with velocity ratio $r = 0.2$ was undertaken to see if this inertial cascade was present close to the fan outlet. At this downstream location, which is well within the region of freestream development where the effects of the individual fans are felt (see Chapter II), a -5/3 region, albeit small, is observed (see fig. 3.29a).

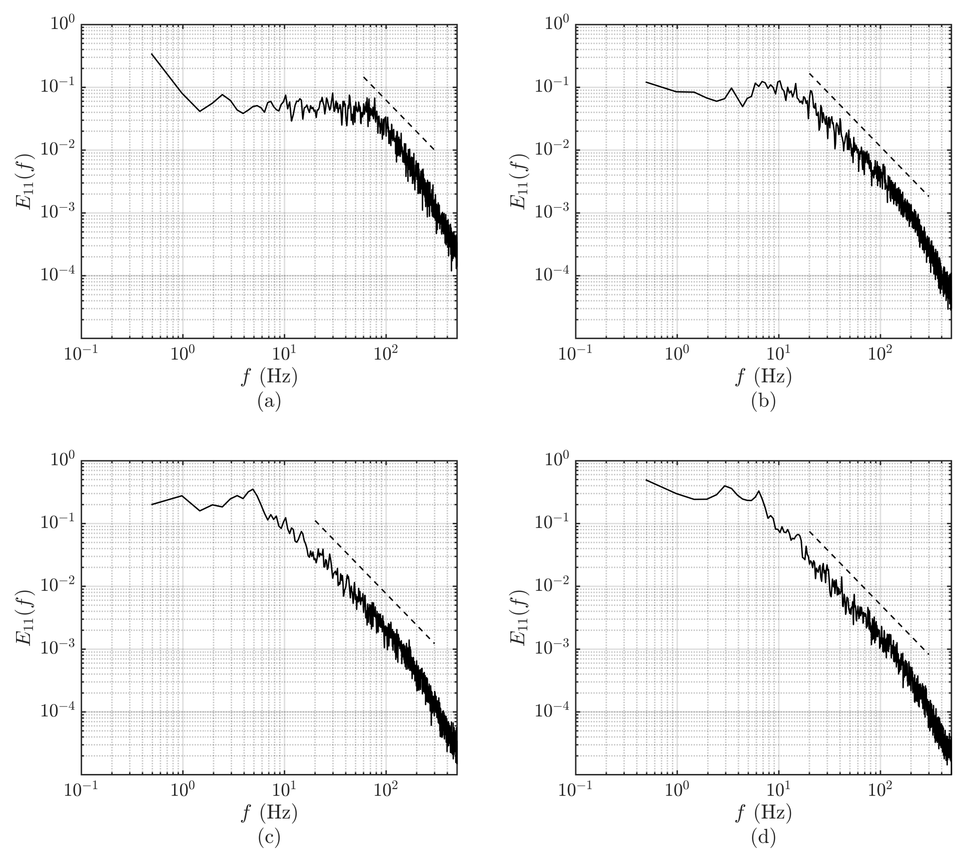

Figure 3.29: Energy spectrum for the dual-stream mixing layer, $r = 0.2$, along the centerline at distances of (a) $x = 7$ inches, (b) $x = 28$ inches, (c) $x = 88$ inches, (d) $x = 118$ inches from the fan array outlet plane. A reference line of slope $-5/3$ indicates a fully developed inertial cascade.

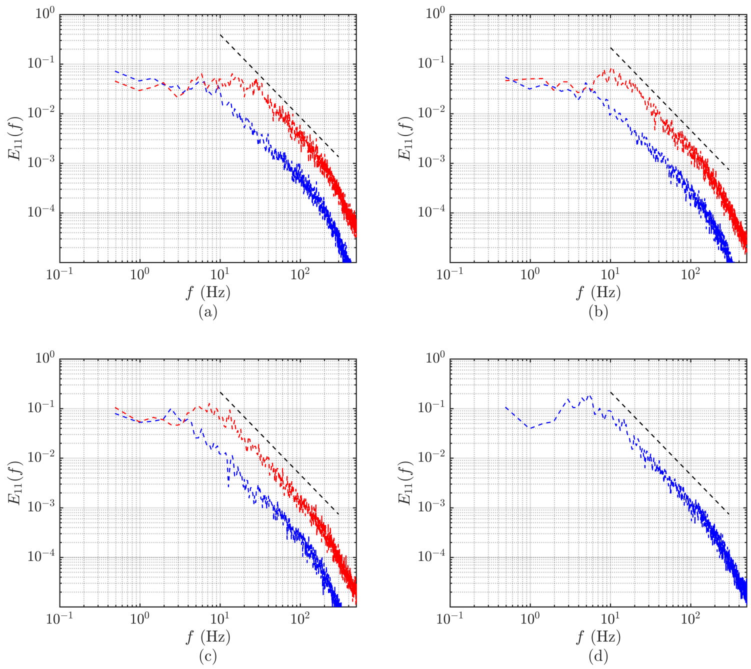

Figure 3.30: Energy spectrum for the triple-stream mixing layer, $ss = 4d$, along the centerline at distances of (a) $x = 28$ inches, (b) $x = 58$ inches, (c) $x = 88$ inches, (d) $x = 118$ inches from the fan array outlet plane. A reference line of slope $-5/3$ indicates a fully developed inertial cascade. Red denotes the upper mixing layer and blue denotes the lower mixing layer.

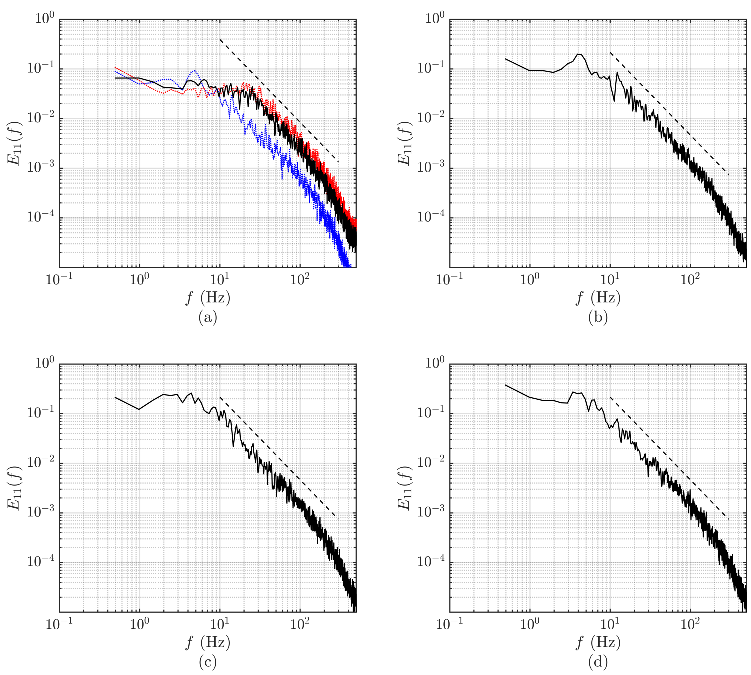

Figure 3.31: Energy spectrum for the triple-stream mixing layer, $ss = 2d$, along the centerline at distances of (a) $x = 28$ inches, (b) $x = 58$ inches, (c) $x = 88$ inches, (d) $x = 118$ inches from the fan array outlet plane. A reference line of slope $-5/3$ indicates a fully developed inertial cascade.

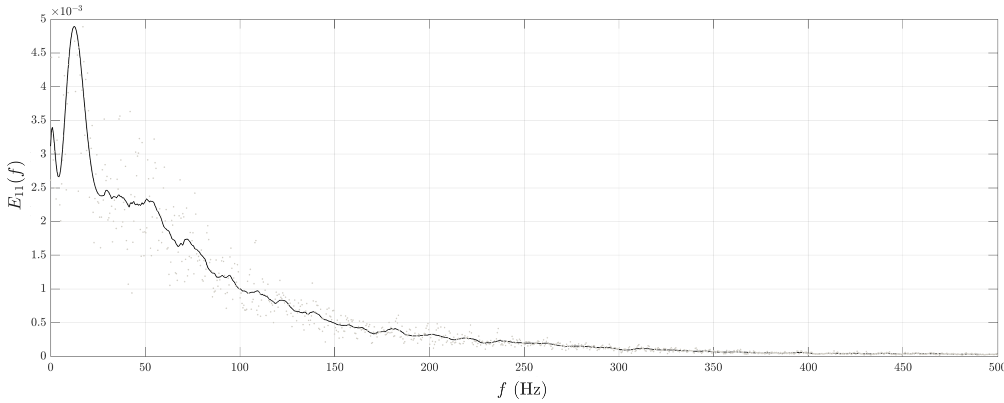

Figure 3.32: Energy spectrum for the dual-stream mixing layer, $r = 0.2$ along the high-speed stream edge at $\eta - \eta^* \sim -1/8$ at $x = 28$ inches distance downstream. A major peak at $f = 12.7$ Hz corresponds to an inverse wave number of 6.3 inches, roughly the non-uniform transverse distance between crests of the spatial wave-front developed from the non-uniform initial conditions of the discrete side-by-side modules.

Energy spectra for the velocity measurements taken just outside the outer edges of the mixing layer, where $\eta - \eta^* \sim \pm 1/8$ is the criteria used to identify the edge (as in Dimotakis and Brown, 1976), can be tracked throughout the flow evolution. Most notable in the earlier development of the mixing layer (e.g. at $x = 28$ inches) is a peak frequency corresponding to an inverse wave number of roughly the module width, an example given in fig. 3.32.

3.4 Fully-developed turbulence - local isotropy

A qualitative difference in the behavior of turbulent shear flows has been noted beyond a transition Reynolds number in outer scales of $Re_{\delta_\omega} \approx 1 - 2 \times 10^4$ (Dimotakis, 2000). This is not to be confused with the laminar/turbulent transition, but is a further transition in the flow observed in many different turbulent flows. It has been suggested somewhat recently by D'Ovidio and Coats (2013) that the underlying growth mechanism of the large structures seemingly changes pre- and post-transition from an amalgamation-event-driven growth mechanism pre-transition to an entrainment-based constant-growth mechanism post-transition. Leaving aside the details underpinning the growth of the large coherent structures, what has been well-established experimentally, numerically, and theoretically post-transition is the change in flow dynamics that manifests as a broader spectrum of eddies with sufficient scale separation to support a quasi-inviscid dynamical representation that is only weakly dependent on Reynolds number. That is to say that post mixing-transition, a power-law regime of slope $\approx -5/3$ emerges in the energy spectrum and broadens with increasing Reynolds number.

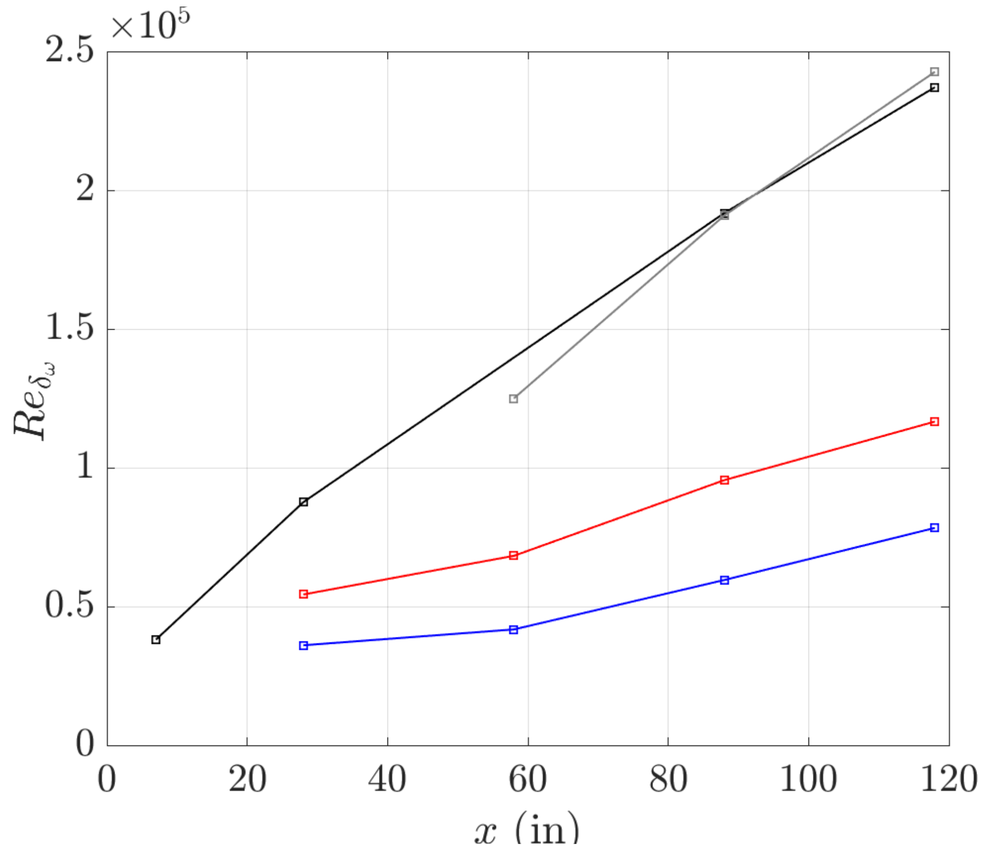

Figure 3.33: The Reynolds number as a function of downstream distance for fully-developed, non-merging mixing layers. The black line is the dual-stream case of $r = 0.2$, the gray line is the post-merged triple stream case with $ss = 2d$ and the red and blue lines are the upper and lower pre-merged mixing layers of the triple-stream case $ss = 4d$.

Because the vorticity thickness scales approximately linearly with downstream distance (i.e. $\delta_\omega(x)$), the local Reynolds number is expected to increase linearly with x. The Reynolds number plotted as a function of downstream distance is given in fig. 3.33. The Reynolds number is well above (oftentimes an order of magnitude higher than) the aforementioned mixing criteria for every data set within the testing domain between $x = 28$ inches and $x = 118$ inches for every mixing layer case presented herein. Even for the traverse taken near the fan outlet plane at $x = 7$ inches is the Reynolds number comfortably above the criteria ($Re_{\delta_\omega} = 4 \cdot 10^4$).

3.5 Summary

This chapter introduced the flow evolutions of dual- and triple-stream mixing layers initiated across a multi-source wind tunnel without the use of a splitterplate geometry. The dual-stream mixing layers were determined to behave principally the same as the canonical single-source splitterplate experiments found in the literature with a noted set of nonuniformities in the outer freestreams attributed to the module geometries that smooth with downstream development. Triple-stream shear layers of varying inter-shear spacings were explored to further elucidate merging characteristics of adjacent shear layers, as this is the primary mechanism of turbulent flowfield generation for nearly every flow modality of multi-source wind tunnels (not implementing flow manipulating geometries). Careful selection of velocity ratios allowed for comparison of post-merged triple-stream mixing layers with their dual-stream counterparts. The shear layer width was accounted for by the vorticity thickness based on the maximum slope of the velocity gradient. The growth of the shear layer was tracked through spanwise traversals at four select downstream locations for velocity ratios $r = 0.2$, $r = 0.4$ such that spreading diagrams could be drawn and virtual origins geometrically determined. When the triple-stream shear layers are initially separated so as to support the evolution of two distinct mixing layers (i.e. $ss = 4d$), the analysis for conventional mixing layers applies. Near-merging and when initialized with a separation distance that does not support two distinct mixing layers (i.e. $ss = 2d$), an augmented analysis based on the parameters of either of the two outermost streams is proposed. Post-merged triple-stream mixing layers recover dual-stream mixing layer type behavior (i.e. the shear layer growth rate appears to recover to the nominal value) with the exception that the shear layer width has necessarily grown by essentially the imposed separation at the array outlet plane. Every configuration tested was determined to be well-above the mixing criteria $Re_{\delta_\omega} > 1 - 2 \times 10^4$. Each of the fully-developed, non-merging mixing layers tested in this experimental campaign is plotted in fig. 3.34. When scaled by the vorticity thickness, non-merging mixing layers have mean velocity profiles that are self-similar even though significant tunnel-related effects were observed in the freestreams. This suggests that the freestream velocity differences, when calculated from values of $\xi = (y - y_{50})/\delta_\omega \sim \pm 1$, are nearly constant with downstream development.

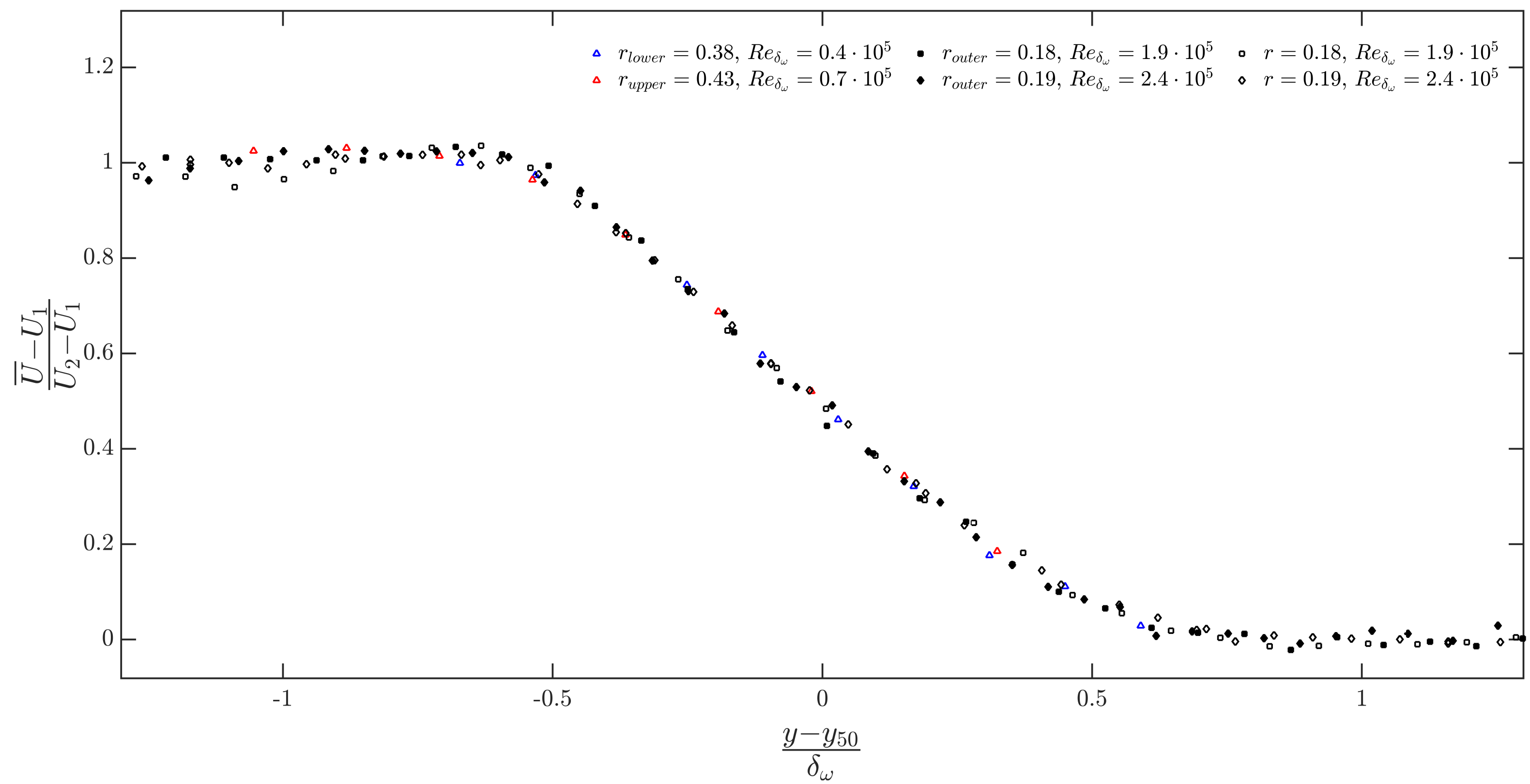

Figure 3.34: Profiles of the nondimensional mean velocity for each fully-developed, non-merging mixing layer.